March 2015

DEVELOPMENT OF INFRARED AND TERAHERTZ BOLOMETERS BASED ON PALLADIUM AND CARBON NANOTUBES USING ROLL TO ROLL PROCESS

Amulya Gullapalli
University of Massachusetts Amherst

DEVELOPMENT OF INFRARED AND TERAHERTZ BOLOMETERS BASED ON PALLADIUM AND CARBON NANOTUBES USING ROLL TO ROLL PROCESS

A Thesis Presented

by

AMULYA GULLAPALLI

Submitted to the Graduate School of the
University of Massachusetts Amherst in partial fulfillment
of the requirements for the degree of

MASTER OF SCIENCE IN ELECTRICAL AND COMPUTER ENGINEERING

FEBRUARY 2015

Electrical and Computer Engineering

DEVELOPMENT OF INFRARED AND TERAHERTZ BOLOMETERS BASED ON PALLADIUM AND CARBON NANOTUBES USING ROLL TO ROLL PROCESS

A Thesis Presented

by

AMULYA GULLAPALLI

Approved as to style and content by the thesis committee:

_____

Sigfrid Yngvesson, Chair

_____

Eric Polizzi, Member

_____

Neal G. Anderson, Member

_____

C. V. Hollot, Department Head
Electrical and Computer Engineering

Dedicated to my mother, father, sister, and to my loving husband

ACKNOWLEDGEMENTS

I want to thank my principal adviser, Dr. Sigfrid Yngvesson, for his guidance during my research and study at Umass, Amherst. I am thankful to him for not only giving me an opportunity to work in his laboratory but also for being a great mentor. He was always accessible and willing to help. His passion and commitment towards research has been very inspirational. Dr. Yngvesson has always been there for me and I could not ask for anything more. This work, of course, would not have been possible without his guidance, inputs, and support. I will forever be thankful to him!

I would also like to thank Professors Eric Polizzi and Neal G. Anderson for the enjoyable learning experience they have provided with the classes. The knowledge I gained from their classes has been very useful during the entire course of my research. I am also thankful to Professor Anderson for helping me during critical times during my Master's first year. I would also like to thank Professor Kenneth Carter for his collaboration with THz laboratory.

Special thanks to CHM Nanofabrication lab manager, John Nicholson, for teaching me everything I know about fabrication. Many times, he went out of his way to ensure we got everything we needed. I would also like thank John for giving me an opportunity to be the lab assistant to CHM. I would like to extend my special thanks to Martin Muthee and Jacob John for their guidance throughout my thesis and also for making lab work fun.

My deepest gratitude goes to my family; my parents Gullapalli Purnanandu and Kameswari, my sister Apurva Gullapalli, my husband Omkar Vyavahare, to my uncle Rampurna Prasad Gullapalli, my mother-in-law Vinaya Vyavahare, and my brothers-in-law Sathish Mandapaka, Kedar Vyavahare and Tushar Vyavahare, and my friend Raghavendra Yerragunta and Shweta Malik for their unflagging love and support. My family has always been there for me. I could not imagine my life without these people.

Finally, I am grateful to all my colleagues and friends whose suggestions and encouragement were invaluable throughout my graduate career at UMass Amherst.

ABSTRACT

Development of Infrared and Terahertz Bolometers Based on Palladium and Carbon Nanotubes Using Roll to Roll Process

FEBRUARY 2015

AMULYA GULLAPALLI

M.S.E.C.E, UNIVERSITY OF MASSACHUSETTS AMHERST

Directed by: Sigfrid Yngvesson

Terahertz region in the electromagnetic spectrum is the region between Infrared and Microwave. As the Terahertz region has both wave and particle nature, it is difficult to make a room temperature, fast, and sensitive detector in this region. In this work, we fabricated a Palladium based IR detector and a CNT based THz bolometer.

In Chapter 1, I give a brief introduction of the Terahertz region, the detectors already available in the market and different techniques I can use to test my detector. In Chapter 2, I explain about the Palladium IR bolometer, the fabrication technique I have used, and then we discuss the performance of the detector. In Chapter 3, I explained about the Roll to Roll based THz bolometer, its working and fabrication techniques, and at the end we discussed its performance.

TABLE OF CONTENTS

Page

LIST OF TABLES

Table **Page**

LIST OF FIGURES

Figure **Page**

CHAPTER 1

INTRODUCTION

1.1 Project motivation

The Terahertz region (THz) of the electromagnetic spectrum is the region between Infrared and Microwaves as shown in Figure 1.1; it typically spans from about 1THz to 30THz, which corresponds to wavelengths from 300µm to 10µm respectively. Frequencies from 100GHz to 1 THz are often called the "Sub-Terahertz" range.

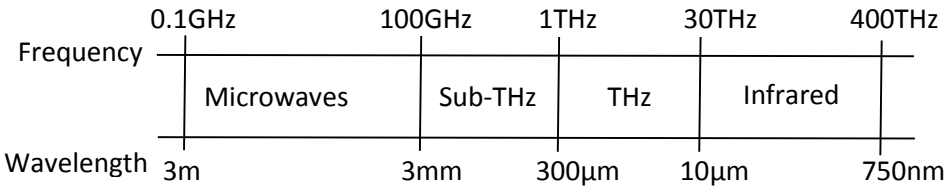

Figure 1.1 Electromagnetic spectrum denoting the terahertz region

Microwave radiation may be considered to have primarily wave nature in most experiments, due to the very small energy of microwave photons, while the Infrared radiation manifests a clearer particle nature. The Terahertz region is the bridge between the classical and quantum mechanical description of the EM waves [2].

The Terahertz radiation is non-ionizing and can penetrate through a variety of non-conducting materials like clothing, paper, cardboard, wood, masonry, plastic, and ceramics [3]. They cannot penetrate through metal and water. Because of all these properties, Terahertz radiation can be used in biology and medical sciences, non-destructive evaluation, homeland security, quality control of food and agricultural products, global environmental monitoring, and ultrafast computing among others [1].

The lack of reliable sources and detectors left the region relatively untouched for several decades. The critical difference between detection at the terahertz frequencies and detection at shorter wavelengths is the low photon energies (1–10 meV), which means that the ambient background thermal noise almost always dominates naturally emitted narrow-band signals requiring either cryogenic cooling of the detector elements or long-integration-time radiometric techniques or both[4]. On the other hand, in comparison to longer wavelength radio techniques, terahertz sensors suffer from a lack of available electronic components—lumped resistors, capacitors, and inductors- as well as amplifiers and low-loss transmission media[4].

This lack of technology led to the THz range being referred to as the “THz gap”. However, this problem is being solved and there are now a variety of sources and detectors available in the market. Silicon bolometers and Superconductor-Insulator-Superconductor devices(SIS) or HEB (Hot Electron Bolometers) are widely available detectors for high sensitivity detection of Terahertz, but the problem with these critical

detectors is that they need to be cooled to a temperature of 4K or below for them to function properly. A lot of work has been done to make a room temperature detector which resulted in the development of Pyroelectric and Golay cell detectors. The problem with this detector is that it is not sensitive enough to detect a small signal. There is therefore a need to develop a room temperature, ultra-fast and sensitive THz detector.

Taking advantage of our group’s expertise, this work will attempt to develop a simple room temperature ultra-fast and sensitive direct THz detector.

Basic definitions to measure the performance of a THz detector:

The calculation of the performance parameters like Sensitivity, Thermal time constant, Noise equivalent power and Thermal conductance helps us to estimate the performance of the detector and also allows us to compare with the performance of detectors already available in the market.

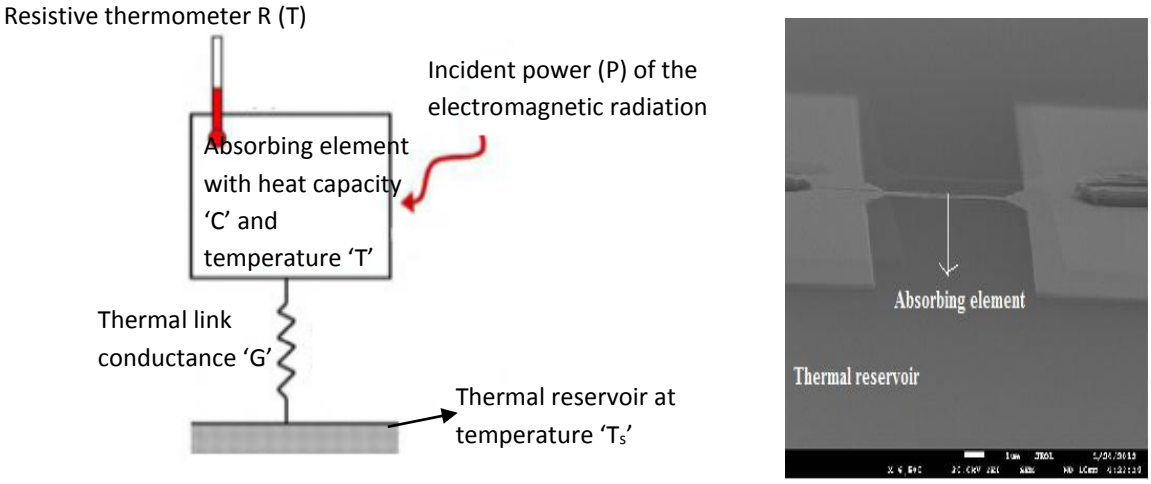

Figure 1.2: Conceptual schematic of a Bolometer (left) and the fabricated Bolometer (right) (The conductance 'G' in the figure is the thermal conductance) [6]

Voltage responsivity (S_V): Voltage responsivity is defined as the ratio of the change in the voltage of the DC biased detector when exposed to the THz radiation to the available Terahertz power from the source (P_{THz}). It denotes the input output gain of the detector. Responsivity is also called sensitivity. Its units are Volts/Watts

(1.1) $$S_v = \frac{\Delta V}{P_{THz}}$$

Intrinsic time constant (τ): This measures the speed at which the signal is detected, i.e how fast the detector can detect the signal. For a Bolometer, it is defined as the ratio of the heat capacity of the absorptive element to the thermal conductance between the absorptive element and the reservoir [5]. From Figure 1.2 the intrinsic time constant can be formulated as

(1.2) $$\tau = \frac{C}{G_{th}}$$

Where C = Heat capacity of the Bolometric element and G_{th}= Thermal conductance G_{th} is defined as $\frac{P_{th}}{\Delta T}$. Here P_{th} is the transmitted thermal power across a device over which a thermal temperature difference of ΔT is applied. As we will discuss later, G_{th} can be obtained for a bolometer by measuring its VI characteristic with a constant current source. G_{th} can then be calculated as follows [7]

(1.3) $$V = \frac{R_0}{1-\beta I^2} I$$

(1.4) $$\beta = \left(\frac{1}{G_{th}}\right) * \left(\frac{dR}{dT}\right)$$

I is the maximum DC current the device could take before the breakdown; it is found from the experimental values. β is called the responsivity coefficient.

S_V is defined as shown in the equation (1.1).From the equations above we also find that

(1.5) $$S_V = \beta * I_0$$

From Equation (1.3) we can calculate the value of β by curve fitting V and I. dR/dT will be calculated from experimental data, by noting the change in resistance for the change in temperature, as the device is placed on a hotplate and probed.

From equation (1.4) and from the measured values of β and dR/dT, we can calcula te G_{th}.

Heat capacity

Heat capacity of any substance is defined as the amount of the heat required to change the temperature of the substance by 1K. The energy supplied will be stored in the electrons and in the ions. Therefore the heat capacity of the substance C = (ϒ*T) (Contributed by energy stored in electrons, Ce) + (A*T3) (Contributed by energy stored in phonons, Cph) [14]. For a first order estimate the energy stored in the phonons can be neglected for the thin film and therefore [14]

(1.6) $C \sim \Upsilon * T$

Noise equivalent power

Noise equivalent power (NEP) is a measure of sensitivity of the detector system or it is the weakest signal that can be detected. It is the power that will produce a signal to noise ratio of 1 in a 1- Hz bandwidth [52]. The NEP at other detection bandwidths scales with the inverse of the square root of the bandwidth.

1.2 Overview of Terahertz detectors

In this section, I will give a short review of some of the most common THz direct detectors and their working principle, performance and limitations. Then, I will introduce two new kinds of THz detectors, which I worked on during my Master's thesis.

Common types of THz detectors

The most common types of THz detectors are

a. Pyroelectric detectors

b. Schottky diodes

c. Semiconductor Bolometer

d. Thermopiles and

e. Golay cells

1.2.1 Pyroelectric detector:

Pyroelectric detector function is a combination of the function of capacitor and generator. It is made of ferroelectric material such as lithium tantalite whose electrical polarization changes with the temperature. When THz radiation is applied to a thin pyroelectric crystal, electric charge is generated by heating and when THz radiation is turned off the crystal cools down and an opposite charge is generated. In Pyroelectric detectors, only modulated radiation creates a signal, so the THz radiation needs to be modulated before detection. When THz radiation hits the detector, a voltage is created across the capacitor and the external impedance. These detectors have several advantages like high responsivity (3-10KV/W), room temperature operation, fast

thermal response (10's of ms), low cost and stability against ambient temperature, atmospheric changes and electromagnetic interference. The drawback for these detectors is that they only respond to the time varying signals and are not sensitive to wavelength, but to the temperature changes.

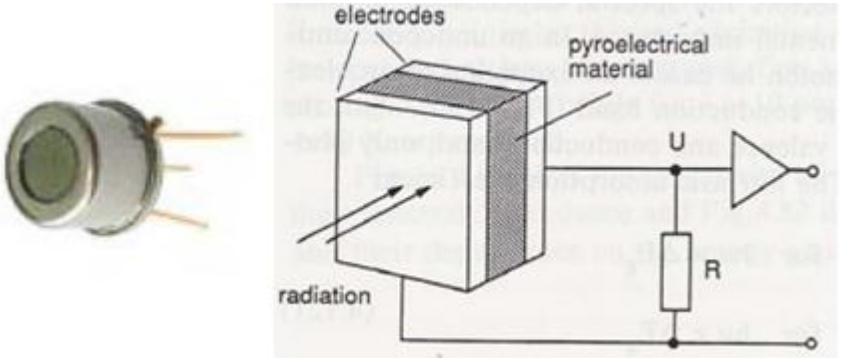

Figure 1.3: Pyroelectric detector

1.2.2 Schottky diode detector

Schottky diodes are commonly used in Microwave and Terahertz frequency ranges as direct detectors and mixers. The Schottky diode detector works by sensing a change in the IV characteristics of the device due to RF voltage applied. In other words, the RF voltage can be detected 'directly' by measuring the changes in the non-linear IV curve of the diode device [23]**.**The current in the Schottky diode is given by equation 1.7.

(1.7) $$I(V) = I_s \,.\, (e^{eV/\eta KBT} - 1) = I_s \,.(e^{\alpha} - 1)$$

When impinged by the RF voltage, V changes to $V_0+\Delta V$

Where V is the voltage across the diode, V_0 is the average DC voltage and ΔV is the oscillating component of the RF voltage. Therefore

(1.8) $$I(V_0+\Delta V) \cong I(V_0) + \frac{dI}{dV}\Delta V + \frac{1}{2}\frac{d^2I}{dV^2}(\Delta V)^2 + \ldots\ldots$$

$I(V_0)$ is the bias current applied to the device

$\frac{dI}{dV}\Delta V$ is the Sinusoidal current varying at the frequency of ω ($V=V_{RF}\sin(\omega t)$)

$\frac{1}{2}\frac{d^2I}{dV^2}(\Delta V)^2$, squared RF voltage and the second derivative of the current is used to detect the RF radiation. This implies the small change in DC current is produced due to the squared RF voltage and is proportional to the RF power.

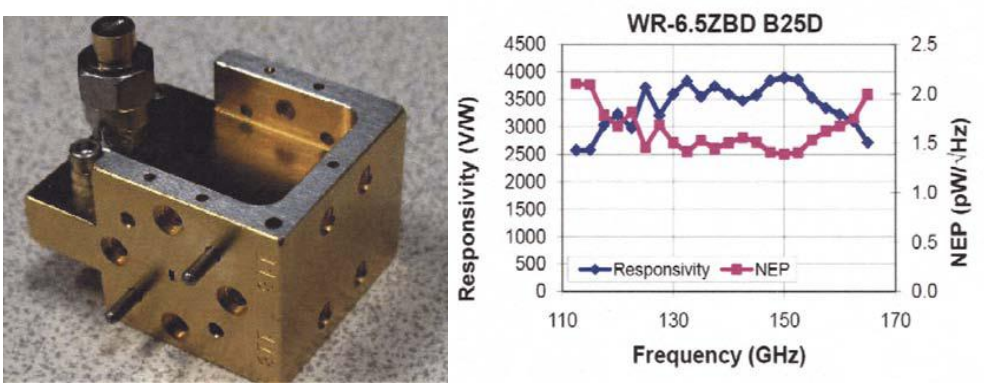

Figure 1.3 Virginia Diode Inc. Zero bias Schottky diode THz detector (left) and responsivity and NEP as a function of frequency (right). Additionally, the detector responsivity ranges from 4 KV/W at 100GHz, to 400V/W at 900GHz; this detector is designed for low power operation with an NEP of about $1.5\times10^{-12}\frac{W}{\sqrt{Hz}}$ [24]

1.2.3 Bolometer

Bolometers are devices used to detect and measure the electromagnetic radiation via changes in the resistance when it is exposed to the radiation. They are also called thermal radiation detectors. The difference between the Bolometric detection and the Schottky diode detection is that in Bolometer the detection is done by RF power absorption while in Schottky diode the detection is done using the instantaneous RF voltage.

There are two models which are proposed to explain the mechanism of the THz detection. The Interband transition model and the Bolometric model [51]. In the Interband transition model, the detection is attributed to the excited electrons and holes which enhance the concentration of the free carriers. But, in the case of the Bolometric model, the energy of the absorbed THz radiation is transferred to the crystal lattice of the sensing element, which results in an increase in its temperature. Therefore the response here comes from the temperature dependence of the resistance.

The bolometer consists of an absorbing element with heat capacity C, connected to a heat sink at a constant temperature, say Ts, through an insulating link of thermal conductance G [5] as shown in figure 1.2

When power is absorbed by the Bolometer, the voltage of the Bolometer changes from V_0 to $V_0+\Delta V$, current changes from I_0 to $I_0-\Delta I$ and the resistance changes from R_0 to $R_0+\Delta R$. Therefore

(1.9) Voltage across the Bolometer $V_0+\Delta V = (I_0-\Delta I) \times (R_0+\Delta R) = I_0R_0+I_0\Delta R-\Delta IR_0- \Delta I\Delta R$

(1.10) The absorbed DC power = $P_{DC}+\Delta P_{DC} = (V_0+\Delta V) \times (I_0-\Delta I) = V_0I_0-V_0\Delta I+\Delta VI_0- \Delta V\Delta I$

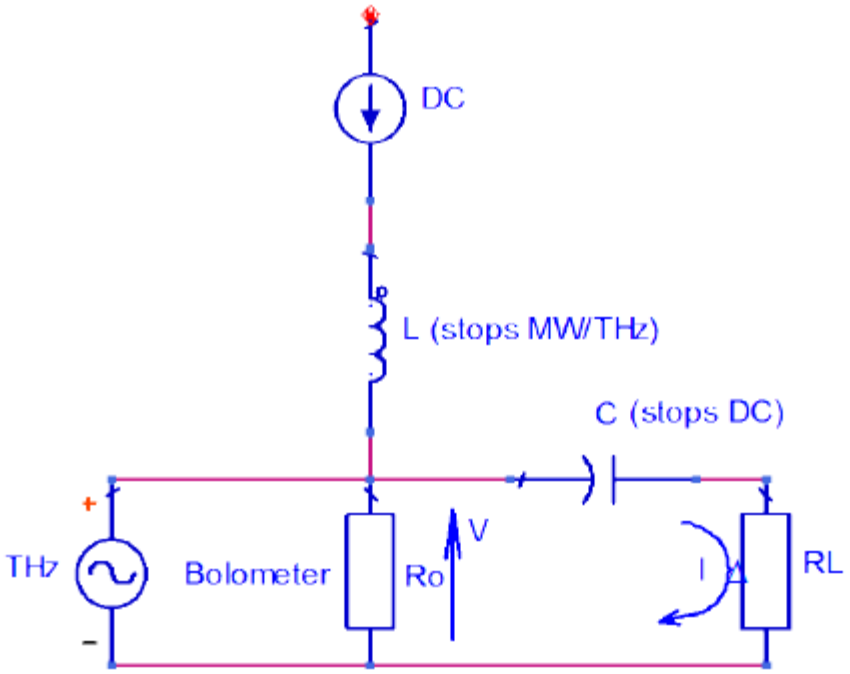

Figure 1.4: Circuit model of typical Bolometer [16]

(1.11) From the circuit above $R_L = \frac{\Delta V}{\Delta I}$

(1.12) The heat capacity $C = \frac{dR}{dP} \cong \frac{\Delta R}{\Delta P} \longrightarrow \Delta R = C * \Delta P = C* (\Delta P_{RF} + \Delta P_{DC})$

The responsivity of the Bolometer is measured by measuring the change in the output voltage for change in the incident power. The responsivity is calculated as follows

(1.13) From equation (1.10), $\Delta P_{DC} = I_0\Delta V-V_0\Delta I$ (Ignoring $\Delta V\Delta I$)

(1.14) From equation (1.11), $\Delta P_{DC} = I_0R_L\Delta I - R_0I_0\Delta I$

(1.15) From equation (1.14), $\Delta P_{DC} = (R_L - R_0)\, I_0\Delta I$

Now from equations (1.9) and (1.11)

(1.16) $\Delta V = I_0 \Delta R - R_0 \Delta I$ (Ignoring $\Delta I \Delta R$)

(1.17) $R_L \Delta I = I_0 \Delta R - R_0 \Delta I$

(1.18) $\Delta I (R_L + R_0) = I_0 \Delta R$

From equation (1.18) and equation (1.12)

(1.19) $\Delta I (R_L + R_0) = I_0 C^* (\Delta P_{RF} + \Delta P_{DC})$

(1.20) From equation 1.15, $\Delta I (R_L + R_0) = I_0 C^* (\Delta P_{RF} + (R_L - R_0) I_0 \Delta I)$

(1.21) From equation (1.20), $\Delta I = I_0 C \Delta P_{RF} * \frac{1}{(R_L + R0) * \frac{1}{(1 - {I_0}^2 C \frac{RL - R0)}{RL + R0}}}$

Note that the denominator goes to zero here when ${I_0}^2 \, C \, \frac{RL - R0)}{RL + R0} = 1$. This phenomenon is termed "electrothermal feedback". For simplicity we will assume that the bolometer is not operated under these conditions.

From the responsivity equation in (1.1)

(1.22) $S_v = \frac{\Delta V}{P_{THz}} \longrightarrow S_v = \Delta I^* R_L * \frac{1}{P_{THz}}$

From equation (1.21), (1.22) and (1.10)

(1.23) Responsivity $S_v = \frac{1}{G_{th}} * \frac{dR}{dT} I_0$ (Ignoring the second order terms)

1.3 Terahertz detection technologies

THz detection can be performed in different ways. The two main detection techniques used are

1. Heterodyne detection technique
2. Direct detection technique

In the lower terahertz bands, heterodyne detectors are generally preferred (although this is very application dependent) and for the shorter wavelengths, direct detectors often offer significant sensitivity advantages [3].

1.3.1 Heterodyne detection:

In the Heterodyne detection technique the radiation is detected by mixing the signal frequency with the radiation of a reference frequency source. The reference source is usually called the local oscillator (f_{LO}), and the output frequency ("IF"; f_{IF} = $|f_{RF}-f_{LO}|$) is the difference between these two frequencies. This method is used at THz frequency when high resolution spectroscopy is needed [4] [8].

Heterodyne detection techniques are used both in single frequency THz systems and in Time Domain Spectroscopy (TDS) THz systems. In single frequency (CW) heterodyne detection the signal and the LO are CW THz waves. The LO has a well-defined single frequency while the signal is either a single frequency or a narrow band of frequencies.

A typical detector element is a GaAs Schottky-barrier diode [15]. The local oscillator acts to increase the output signal beyond that obtained in direct detectors,

and heterodyne detectors are therefore in general more sensitive than direct detectors. Bolometers can also be used as heterodyne detectors [9].

1.3.2 Direct detection technique:

Direct detectors are rapidly encroaching into the realm of heterodyne systems for applications that do not require ultrahigh spectral resolution [3].This kind of detection technique is used in Microbolometers, Golay cells (an acoustic bolometer), fast calorimeter, pyroelectric detector etc. [3]. Beyond 1THz, it is often preferred to use the Direct detection technique [3], since suitable LO sources are scarce or expensive. We study Microbolometers in this thesis.

In the Direct detection technique the radiation from the source is directly detected without mixing it with the signal from a local oscillator. As the THz signal intensity is so small, we need a detection technique to be very sensitive. As the Direct detection technique has moderately high sensitivity and broad frequency coverage this method is used for detecting the signal [10]. In this method we align the device, which is DC biased, directly in front of the source and monitor the change in the resistance when the device is exposed to the radiation.

CHAPTER 2

PALLADIUM INFRARED BOLOMETER

2.1 A brief overview of designing and testing of palladium bolometer

The Bolometer made in this thesis work has a thin layer (~40nm) of Pd on an oxidized Si wafer. The Pd strip works as an absorbing element, the SiO2 as the insulating link and Si as the heat sink. When the radiation is impinged on the absorbing element (the Pd strip), it absorbs the radiation and converts it into heat and increases its temperature from its initial temperature (T) above the thermal reservoir's temperature. The temperature dependence properties of the 40nm thick Pd are studied and will be discussed in the following section. Similar bolometers were earlier developed that employ Niobium [7] and Platinum [12].

We take advantage of the characteristic that as the voltage is increased the temperature of the bolometer is increased. The behavior of the bolometer for a change in the temperature by changing the voltage should be similar to the change when the temperature is changed by impinging the terahertz radiation. When the voltage is increased (the temperature increases) the resistance changes in an approximately Parabolic fashion as shown in the Figure 2.1

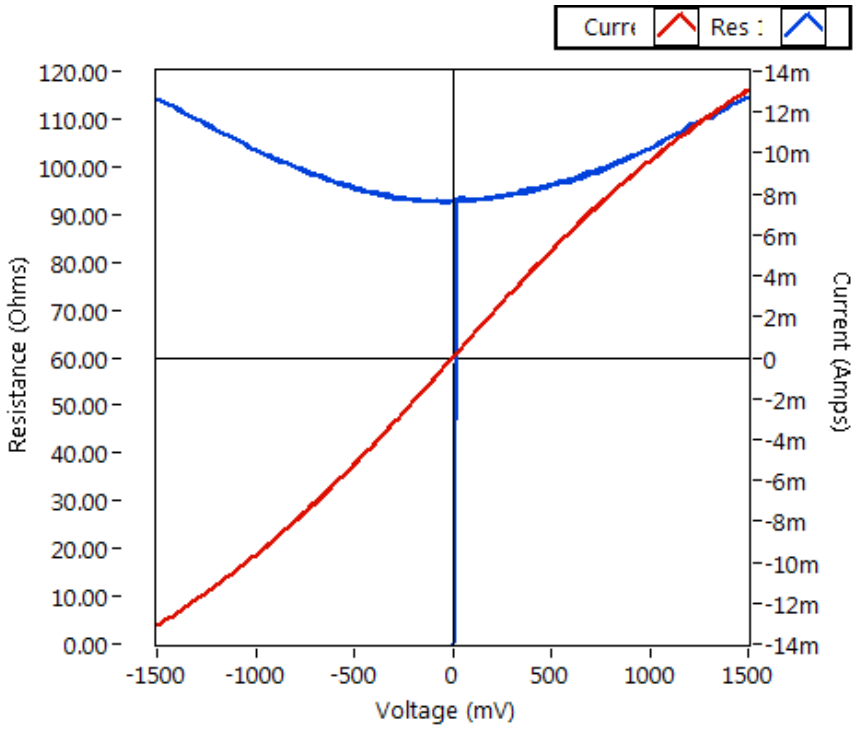

Figure 2.1: DC characteristics of the Pd Bolometer. This DC characteristic can be used as an indicator that the Bolometer will detect the EM radiation.

The graph above indicates that the device can detect the EM radiation. It will work for EM radiation of any frequency which can be absorbed by the Pd film. In practice this means that the Bolometer will operate into the Visible light region. In this thesis we will test the Pd Bolometer at near infrared and THz frequencies.

In the following sections we will discuss how the material is selected, and also how the bolometer is designed and tested.

2.2 Material selection:

Our group has a wide experience in fabricating heterodyne Terahertz Bolometer using Niobium nitride. As Niobium has been proved to be a good material for a THz Bolometer at cryogenic temperature [7], we started fabricating the Bolometer with

Niobium. But Niobium gets oxidized at room temperature and makes very bad contact with the Palladium antennas and this also creates a huge contact barrier which has to be overcome at room temperature. Because of this limitation we were not able to proceed further with the Niobium Bolometer.

To fabricate a room temperature Terahertz Bolometer, we have chosen a thin layer of metal which has sufficient $\frac{dR}{dT}$ to work as a bolometer. Thin films of Pd also have a higher resistivity than Au or other metals for a reasonable size to match the resistance of the THz antennas.

Also, in the paper referenced in [12], that group has fabricated a room temperature infrared sensor with Platinum nano wires. Platinum and Palladium do not oxidize. This property helps us to achieve better Bolometric characteristics at room temperature. As the Palladium and Platinum belong to the same group in the periodic table they should have similar properties for Electromagnetic radiation. Platinum being more expensive than Palladium, I have decided to work on making a room temperature Palladium Terahertz bolometer, by designing an appropriate antenna for THz sensing. As Gold is considered to make a very good electrical contact, it is used for the contact pads.

2.3 Antenna and Bolometer design:

In the Palladium Terahertz bolometer, the absorbing element is placed in the gap of an antenna. We have worked on different kinds of antennas as shown in the figure 2.2. Bowtie and extended Bowtie antennas can be used to pick wide frequency ranges, whereas the patch antenna is designed to be used at particular frequency range.

In the reference [12], the team did not actually have a separate antenna fabricated because for the IR detection the antenna size required is comparatively very small, and the nano wires are so small that the bolometer itself worked as an antenna. But for the Terahertz detection the antenna has a considerable size compared to the bolometer and can be designed well to resonate at 1.9THz (the frequency of the THz laser source). We have tried using different antenna designs, shown in Figure 2.2 (not to scale).

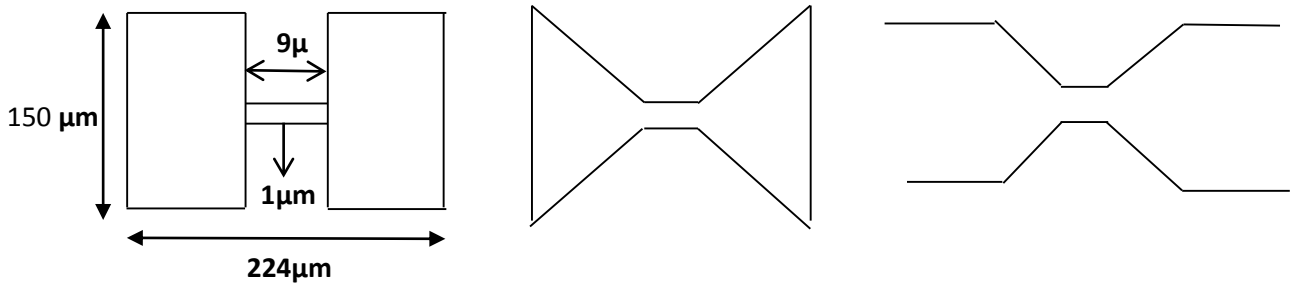

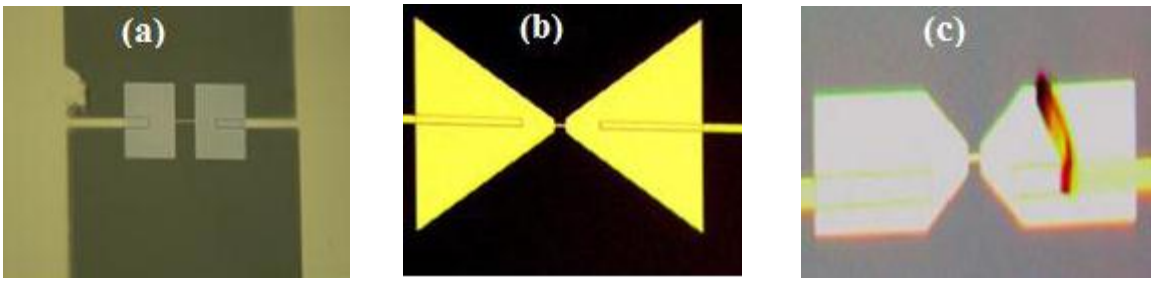

(a) Double Patch antenna (b) Bowtie antenna (c) Extended Bowtie antenna

Figure 2.2 Different types of antenna designs used

The antenna is designed based on the theory explained below

(2.1) Antenna length (λ) = $\frac{\text{Free space wavelength } (\lambda_0)}{2\sqrt{\varepsilon_{\text{eff}}}}$

Where $\varepsilon_{eff} = \frac{\varepsilon_{si}+\varepsilon_{air}}{2}$, and ε_{si}= 11.5 [19]; therefore ε_{eff}=6.25

Based on the above calculation, the length of the antenna is equal to 224µm and width is equal to 150µm. For Bowtie and extended Bowtie antennas, the size need not be precise.

Based on the private communication with Martin Muthee of THz laboratory at UMass, Amherst, the double patch antenna radiates from the slot between the two patches. The slot should be designed to have the same length as given for the bow-tie antenna above. The thickness of the antenna is chosen to be the minimum possible thickness of palladium using the evaporator and Sputtering machine in the cleanroom, which is 40nm.

2.4 Fabrication:

The device is fabricated on a High resistivity Silicon substrate. High resistivity Si behaves as a low loss medium for THz. Due to its lack of donors it has low absorptive losses, and also due to its large direct band gap, prevents THz photons from being absorbed across the band gap [16]. Even though the wafers have high resistivity, when they were probed they showed a finite resistance, which might affect measurements of the resistance of the Bolometer. So, the device is oxidized to a thickness of 300nm using Plasma Enhanced Chemical Vapor Deposition (PECVD). The Ebeam Lithography process is then used to define the contact pads on a PMMA2 spun, oxidized, high resistivity wafer dice as shown in the Figure 2.3.

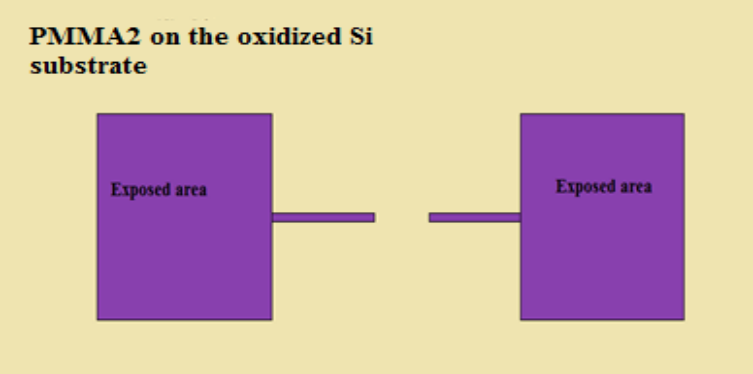

Figure 2.3: The figure showing the contacts after EBL process. Blue indicates the exposed area

Following this is the metallization step in which ~10nm of Titanium and ~100nm of Gold were evaporated using the Ebeam evaporator system. After the Liftoff the device is spun again with PMMA2 and the pattern of the antenna and the Bolometer is defined using the Ebeam writing process. This step is followed by the metallization step in which ~10nm of Titanium and 60nm of Palladium is evaporated using the Ebeam evaporator system. After the liftoff, the device is ready to be tested for its DC and THz detection characteristics. The final device is as shown in Figure 2.4.

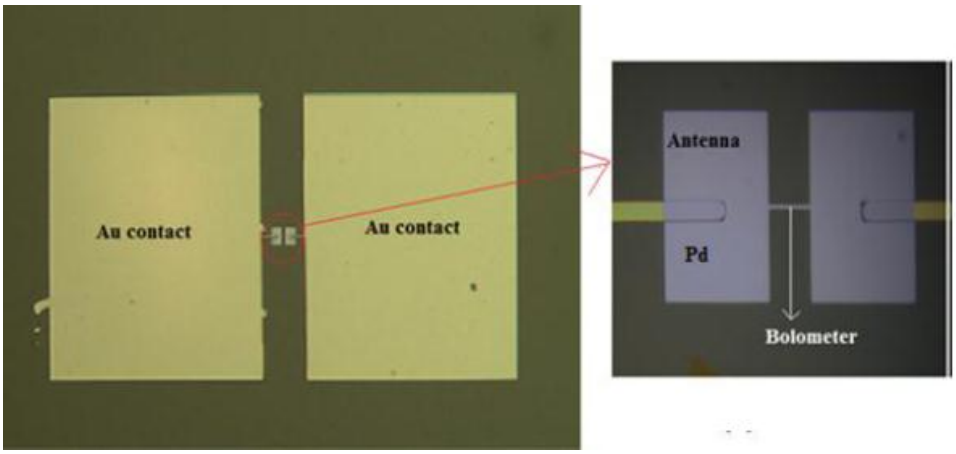

(a) **(b)**

Figure 2.4: (a) Optical image of the complete device with the patch antenna design (b) Optical image of the double patch antenna design.

The procedure of the fabrication is summarized in the flow chart shown in Figure 2.5

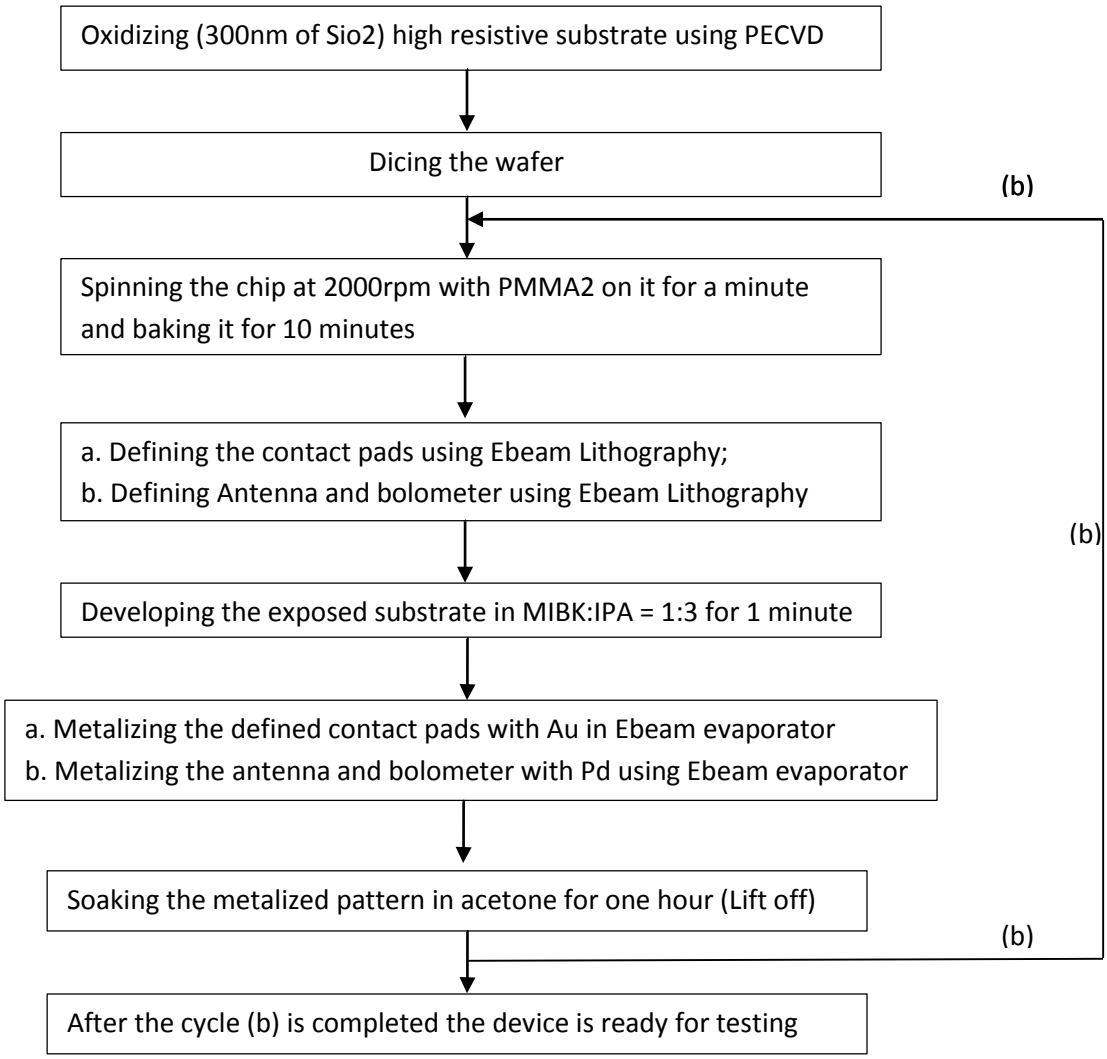

Figure 2.5: Flow chart summarizing the Fabrication process

2.5 Experimental techniques

The testing is done to study DC, THz and Infrared radiation detection characteristics.

2.5.1 Testing of the DC characteristics

The DC characteristics of the device are measured by using a two probe measurement set up. The voltage is applied to the device through the gold contacts, using the Source Measuring Unit (SMU) and the current through the device is measured simultaneously. Keithley 2600/ 2400 is used for sourcing and measurement, and is controlled by the LABVIEW program.

2.5.2 Testing of the THz detection

The THz detection is done using the direct detection technique, which was explained in section 1.3.2. The basic principle for the detection is that, when the modulated THz signal is impinged on the detector element, which was already biased, there will be a voltage difference. The THz source used is a CO_2 laser pumped far infra-red (FIR) gas laser, which our team has been using for the past several years, as shown in Figure 2.7.

The THz source, our team named it as SIMON, is a cascade of the two lasers mentioned above and can be operated at one of many frequencies by changing the gases in the FIR tube and by adjusting the Laser tube length [17]. The CO_2 laser can also be operated at the range of different frequencies of which a particular one is chosen to pump the gas in the FIR tube. The source is continuously supplied with the chilled water to ensure proper functioning. The output of the CO_2 laser is directed by the mirror arrangements to the FIR input. The FIR tube is filled with Difluoromethane gas and the

pressure in the tube is maintained around 80mTorr to get good signal at the output of the FIR laser. The Pyroelectric Detector is used at the output of the FIR laser to ensure that the THz signal could be seen at the output. The FIR laser needs to be chopped since the Pyro electric detector does not respond to continuous wave radiation.

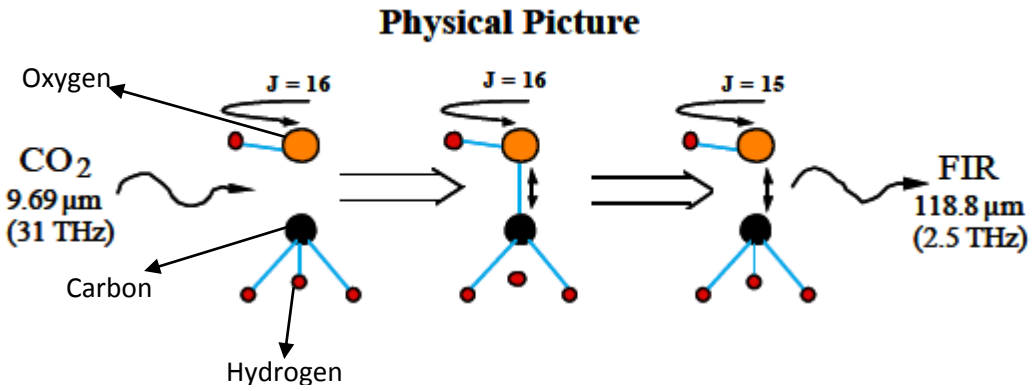

Figure 2.6: The chemical reaction that happen in the FIR tube to produce the Terahertz radiation (an example to produce 2.5THz line) [26].The gas in the FIR tube in my experiment is CH_2F_2 (Difluoromethane) which produces 1.9THz at the output.

When an IR photon with energy closely matches a rotational state at ground energy level to excited vibrational manifold is absorbed by gas molecule, population inversion between rotational states occurs and emits Terahertz radiation [26].

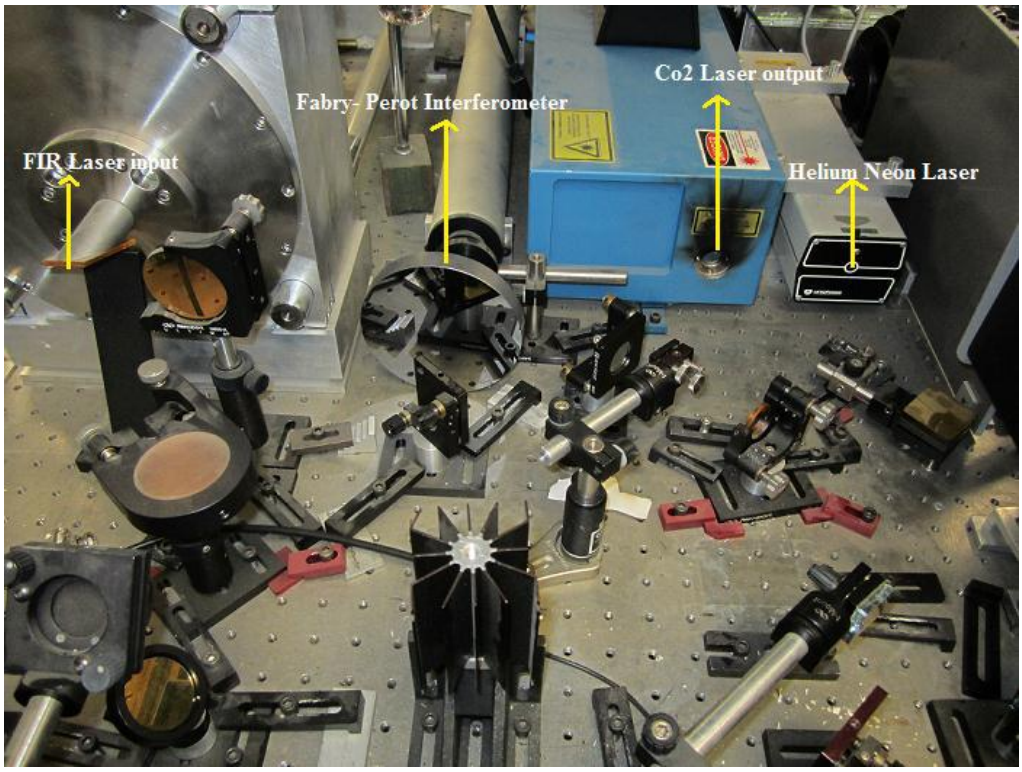

Figure 2.7: THz laser setup

The wavelength of the CO_2 laser is approximately 10µm and the power is 30W [17]. This along with the 9P2 tuning of the CO_2 laser creates a roughly 1mW beam of frequency of 1.9THz, polarized perpendicular to the optical bench [17]. We used the FIR laser with difluoromethane gas.

As the Bolometer is very small and the beam follows a Gaussian form, a method is needed that can couple the Bolometer efficiently to the laser source. Therefore a high resistivity silicon lens is glued to the back side of the chip for directing all the radiation to the antennas and the Bolometer. Bees wax is used to stick the lens to the chip as it is transparent to the THz radiation. The lens is attached as shown in Figure 2.8, to focus the THz radiation to the device and the antennas would pick up the signal and convert it into THz currents.

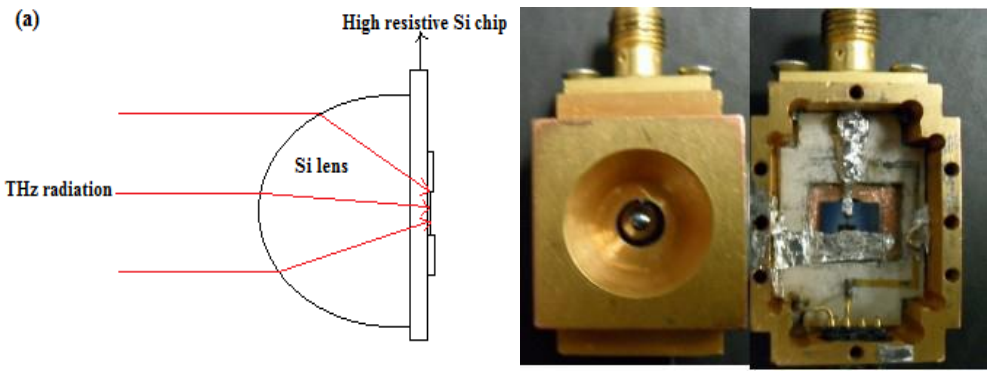

Figure 2.8: (a) THz beam pattern through the Si lens (left) (b) Si lens mounted on the device (right)

These currents travel to the Bolometric strip and heat it. The resulting change in the resistance can be measured. This device is fixed in a SMA connector equipped block and mounted using Indium foil for connections.

From our group's experience with the Silicon lens, a 3dB loss in THz power is expected at the Si lens and 1dB loss in a thin film of Zitex, which was attached to prevent the detection of radiation higher than ~6THz frequencies [18]. As our source is powerful enough the 4dB loss in total can be tolerated.

The THz signal is modulated by using an Acousto-optic modulator (AOM) or a mechanical chopper. The detection is tested by placing the block with the device, with lens facing the signal at the output of the FIR by connecting the device to the Keithley and monitoring the change in detected signal with the modulation.

2.6 Results and discussion

2.6.1 DC Characteristics

The DC characteristics of the device are studied using the two probe measurement explained in the section 2.5.1.

2.6.1.2 Niobium Bolometer

The Bolometer needs to be ~100Ω in resistance, to match with the antenna impedance. The Nb Bolometer has been fabricated with different dimensions to achieve this resistance.

1. Bolometer with 9µ in length and 5µ in width

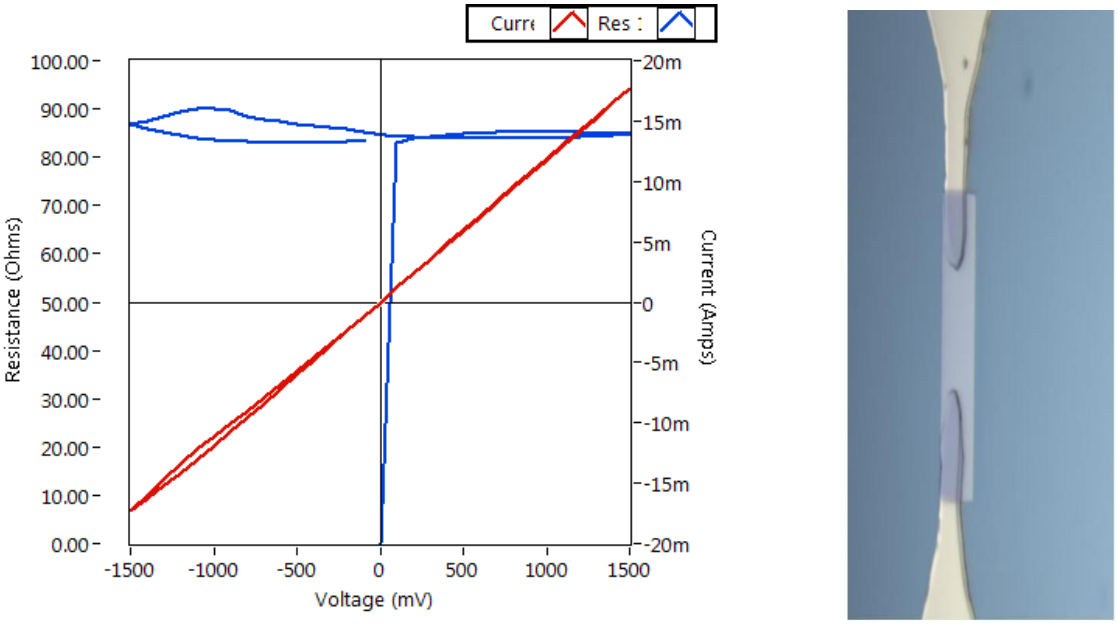

Figure 2.9: DC characteristics (left) and the Nb Bolometer of 9µm*5µm dimensions (right)

For good bolometric characteristics the resistance is expected to change considerably with a change in the voltage but for the 9 µm Bolometer shown in the figure the resistance remains almost the same with change in the Voltage which shows that it is a not a good Bolometer.

When the device size has been changed to 1.5µm by 5µm, the resistance is ~300Ω and when the antennas are fabricated it decreased to 90Ω at 1500mV as shown in the Figure 2.10

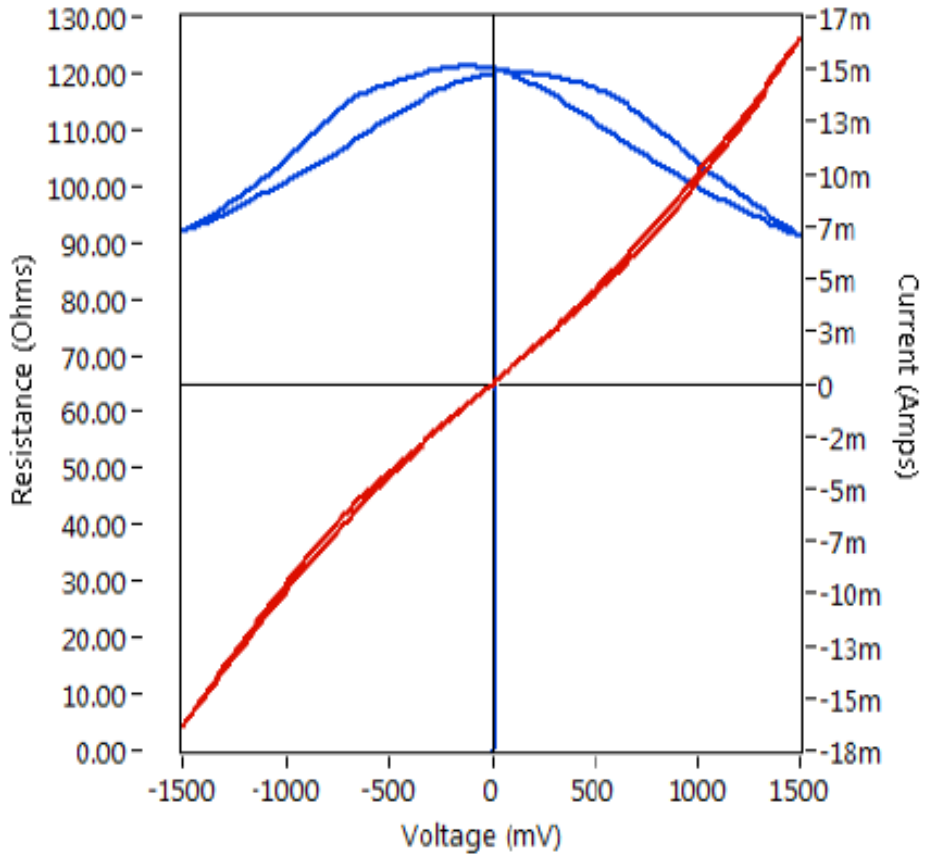

Figure 2.10: Change in resistance with change in voltage

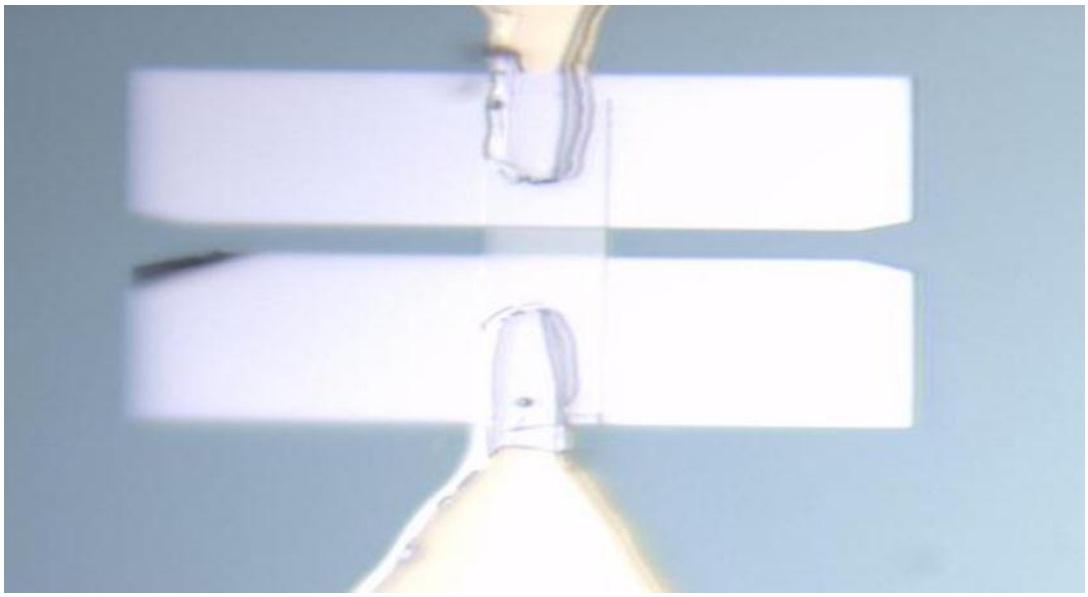

Figure 2.11: Nb bolometer of 1.5µm*5µm dimensions

The problem with these devices is that there is a considerable amount of contact resistance between the Au bars and the Nb Bolometer (which could be seen from the concave VR graph), because of the oxidization of Nb. Because of these limitations, we chose a metal Pd which has been proven to detect electromagnetic radiation.

The Niobium Bolometer is concluded to be an inferior THz detector from its DC Characteristics. As the power output of SIMON is very small, there has been no significant detection of the THz radiation observed in the Nb Bolometer. It is mainly dominated by the noise.

2.6.1.3 Palladium bolometer

The bolometer is fabricated in a continuous strip along with antennas in a one step process. The Pd bolometer has size of 10µm by 1µm and its DC characteristics are shown in the figure 2.12

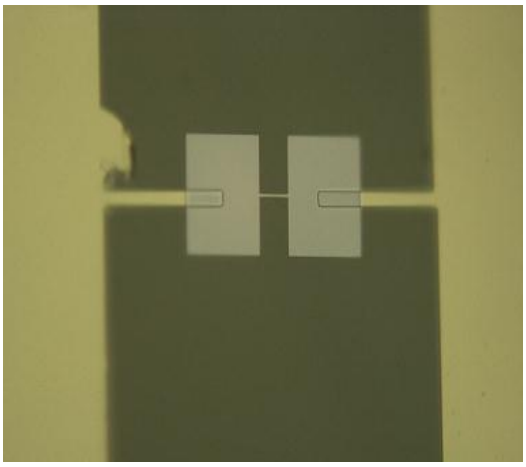

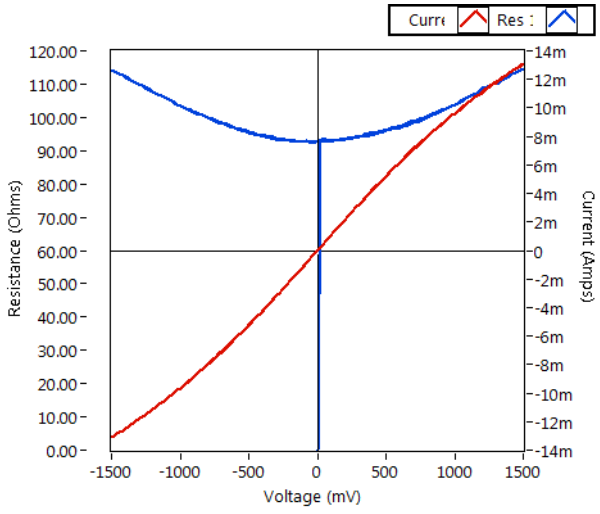

(a) and (d)

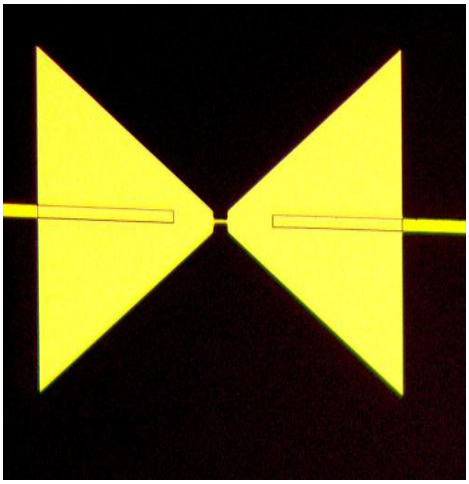

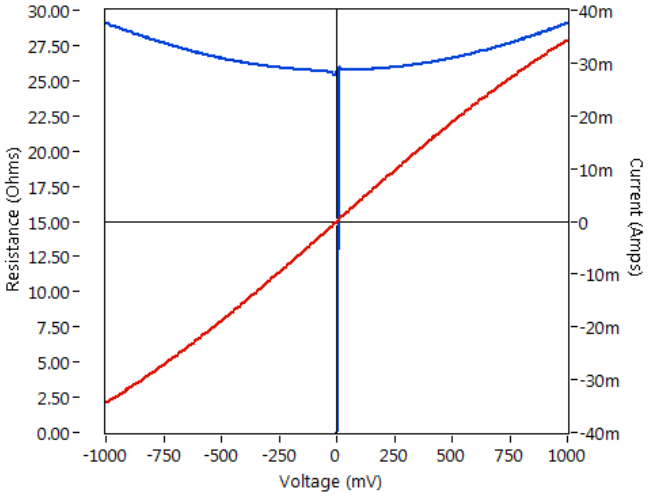

(b) and (e)

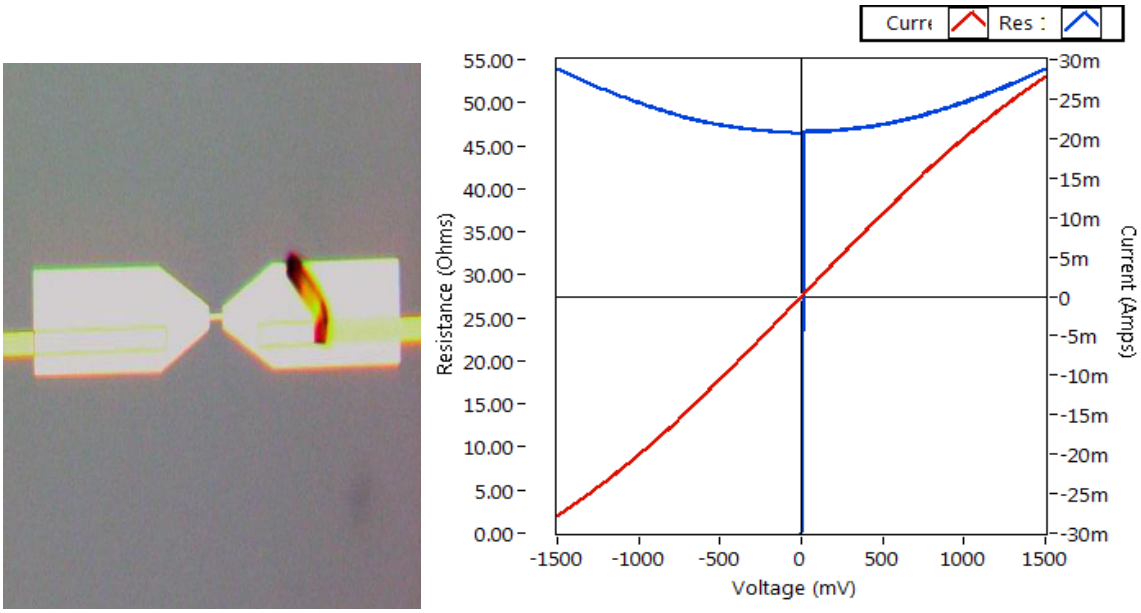

(c) and (f)

Figure 2.12: Pd Bolometer (a) with Patch antenna (b) with Bowtie antenna (c) With extended Bowtie antenna. DC Characteristics with (d) Patch antenna (e) Bowtie antenna (f) extended Bowtie antenna

2.6.2 THz and Infrared detection results:

ϒ for Pd = $9.42*10^{-3}$ J/mol K^2 [14]; 1 mole of Pd = 106.42 gm [13] The Volume of the Pd Bolometric strip (V) = 10µ*1µ*60nm= $6*10^{-13}$ cm^3

The density of Pd (ρ) = 12.02gm/cm^3 at 293K [13]

Therefore the weight of the Bolometric Pd strip = $12.02*6*10^{-13}$gm. = $72.12*10^{-13}$ gm

ϒ for 106.42 gm = $9.42*10^{-3}$ J/ K^2

Therefore ϒ for $72.12*10^{-13}$gm = $6.38*10^{-16}$ J/K^2

The Heat capacity for the strip at 293K is Ce = $6.38*10^{-16}*293 = 1.87*10^{-13}$J/K

Given Ce and G_{th}, we can now calculate the intrinsic time constant (τ)

2.6.2.1 Palladium Bolometer

The significant change in the resistance with change in voltage in the DC Characteristics shown in the figure 2.12 is an indication of a good potential for bolometric detection. The antenna design mainly determines which frequency range of EM radiation is detected. The different antenna designs shown in Figure 2.12 have proved to detect different frequency ranges in other words.

The three different antennas shown in Figure 2.12 are tested for the Infrared detection with the help of a LED source of 940nm wavelength (peak wavelength) and the output power of 20mW [20].

Detection experiments:

The detection when the LED source is being modulated by function generator at a frequency of 50 mHz, is shown in the figure 2.14a. The Responsivity (Sv/R) is calculated as explained below

ΔI is obtained from the graph and ΔV = ΔI* R

The LED source power = 20mW (as measured by the Scientific power meter)

We now assume that the LED has an approximately Gaussian beam based on web data for similar LEDs [17]. The LED has a built-in lens and the radiation pattern has half power points at angles of about 0.1 radians. At an estimated distance of 1.5 mm from the LED this corresponds to a radius of 0.1*1.5 mm = 0.15 mm. At this radius

$$e^{-\frac{r^2}{w^2}} = 0.5$$ from which w =0.618 mm.

We next assume that the device area can be assumed to be circular with a radius 'a' and

$\Pi a^2 = 1.2 \longrightarrow a = 0.618\text{mm}$

From equation 2.26 in [17], Power transmitted through a circular aperture near the axis with radius a is given by

$$P_{device} = P_{LED} * \frac{2}{\pi w^2} \int 2\pi r e^{\frac{-2r^2}{w^2}} dr = (1 - e^{\frac{-2a^2}{w^2}}) * P_{LED} \qquad [17]$$

Therefore P_{device} = 20mW (1-$e^{-0.00017672}$) = 0.000176*20mW = 0.003534mW

Therefore Sv = $\frac{\Delta V}{0.003534\text{mW}}$ .Note that only a small fraction of the LED power impinged on the active device area.

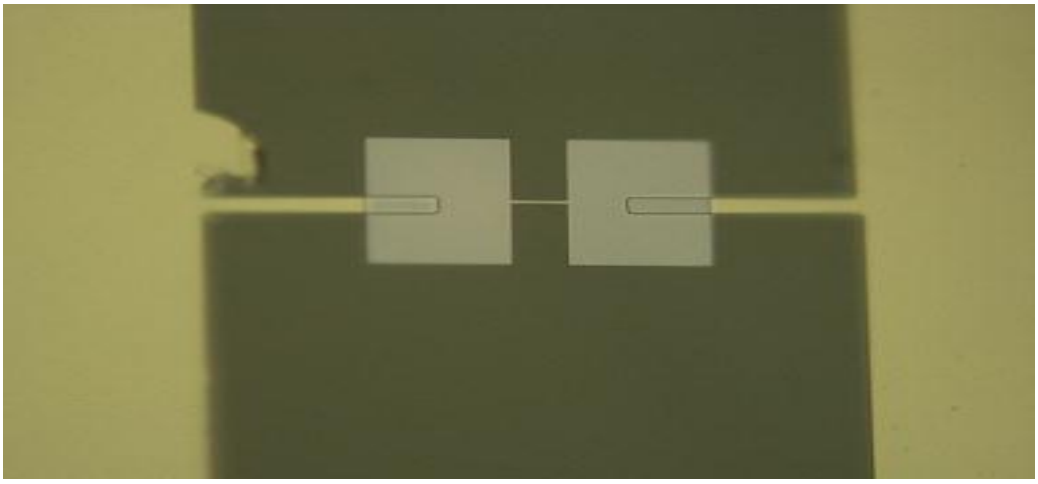

Figure 2.13: The THz bolometer with the patch antenna

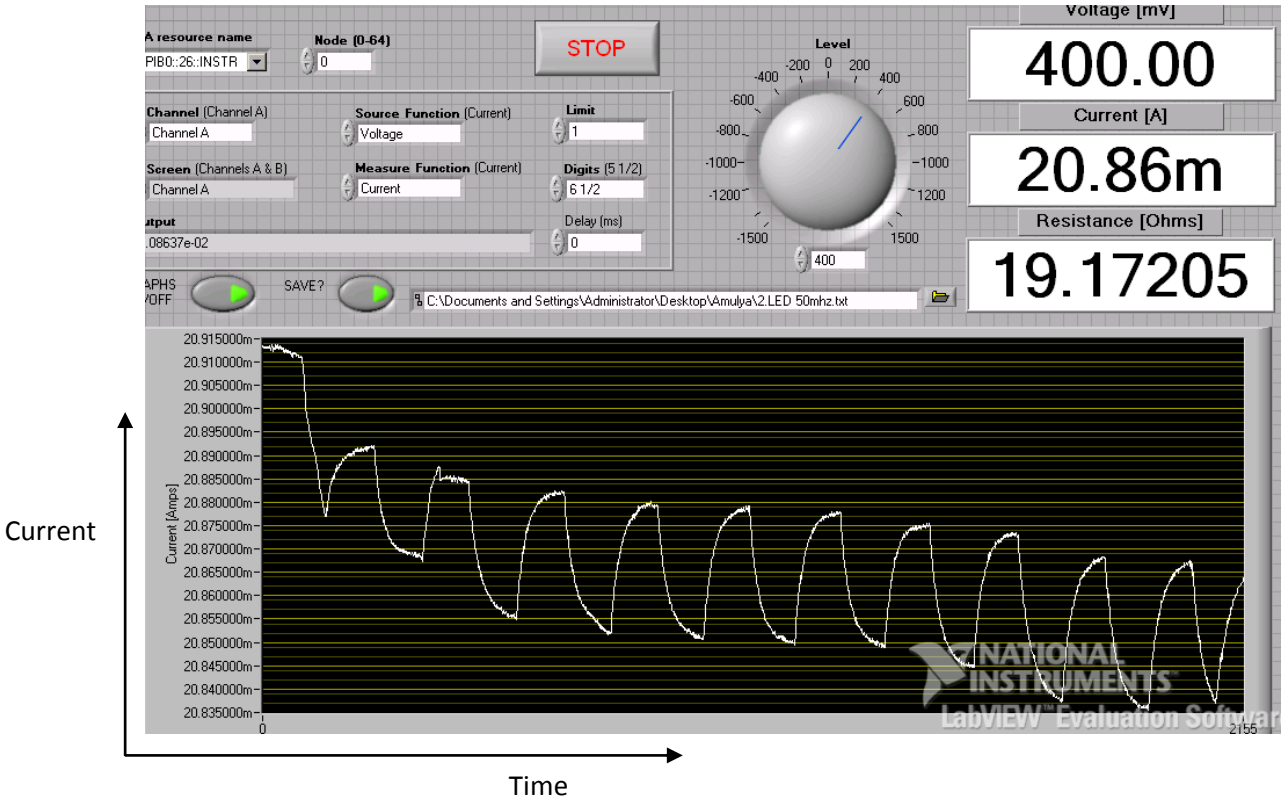

Figure 2.14(a): At 50 mHz; Δ I=20.874-20.836=0.038mA; Δv=0.7285mV, R = 206 V/W

There are several devices fabricated with the above mentioned design. Patch antenna design is used below to show the sample calculation.

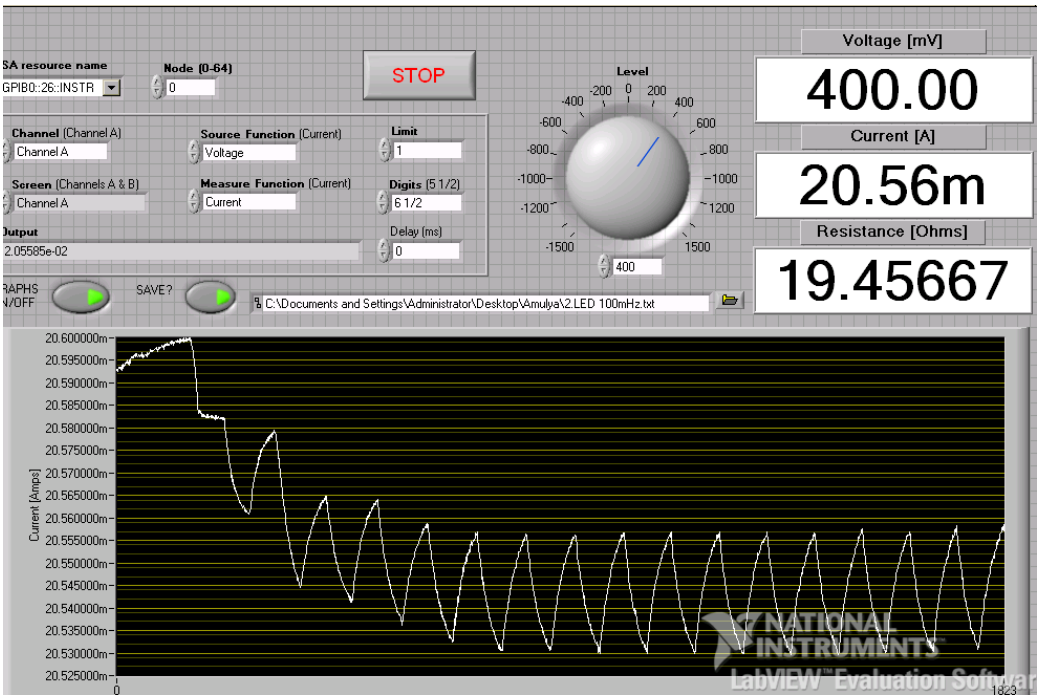

Figure 2.14(b): At 100mHz, ΔI= 20.5555-20.53=0.0255mA; ΔV=0.4961mV, R= 140V/W

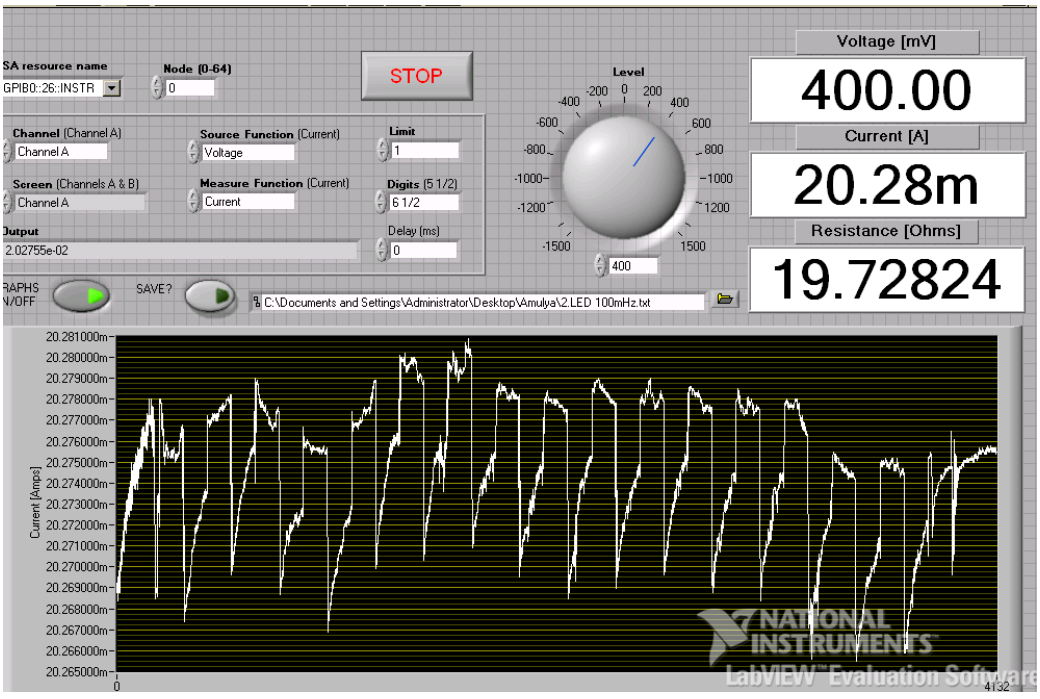

Figure 2.14(c): At 200 mHz; ΔI= 20.275-20.266=0.009mA; ΔV= 0.17755mV, R= 50V/W

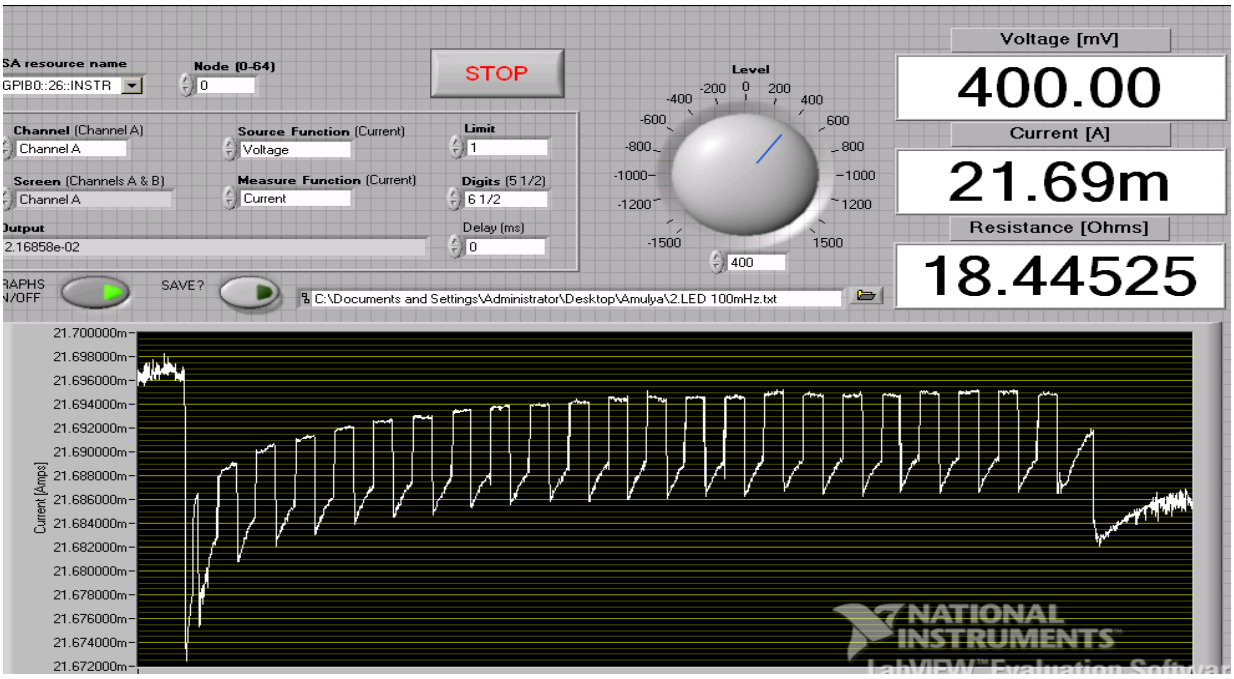

Figure 2.14(d): At 500 mHz; ΔI = 21.694-21.686=0.008mA; ΔV=0.1475mV; R= 41V/W

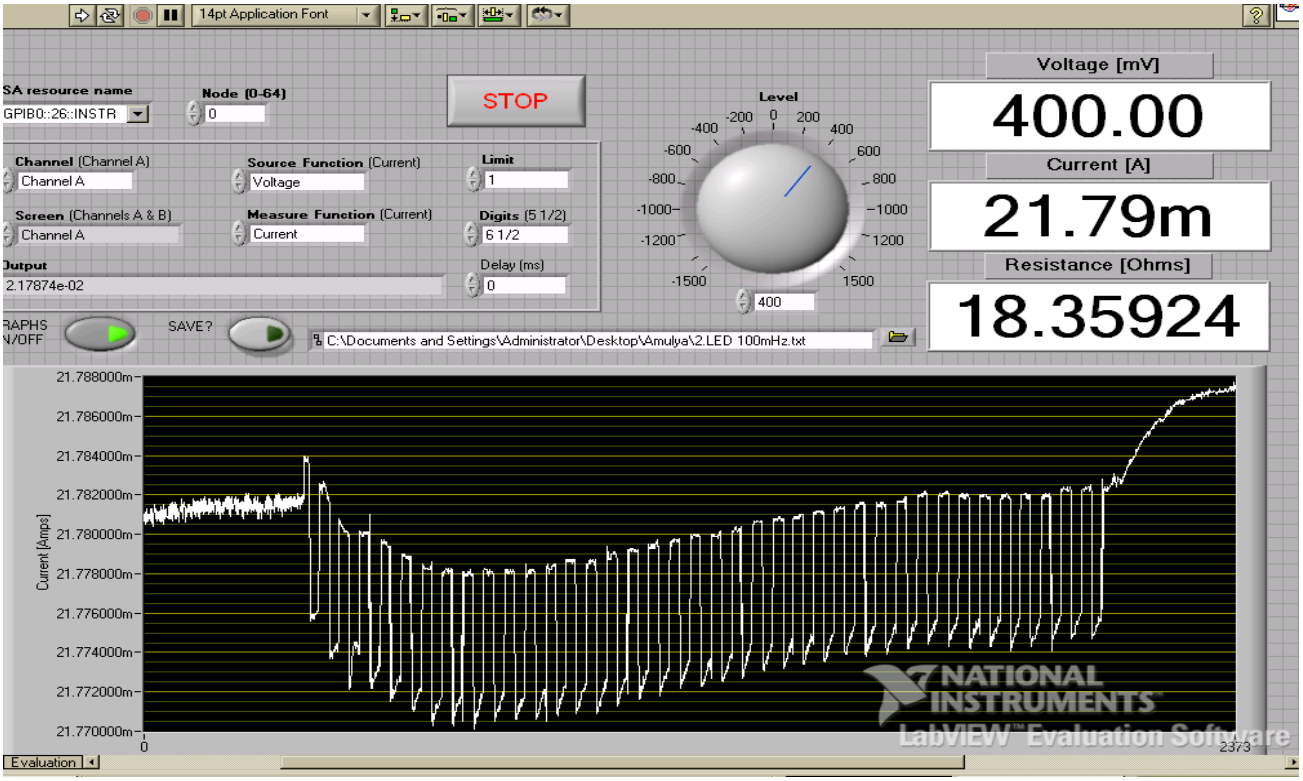

Figure 2.14(e): At 1Hz; ΔI=21.782-21.774=0.008; ΔV =0.1468mV; R= 41V/W

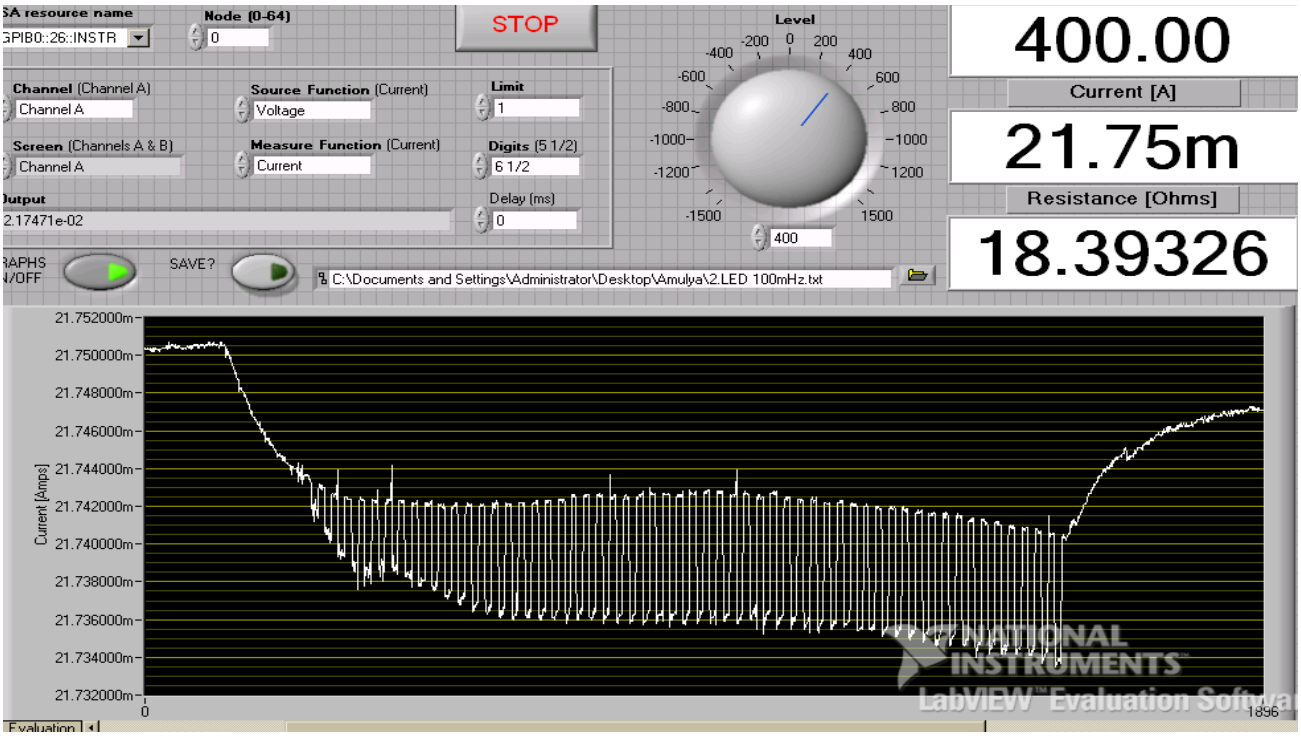

Figure 2.14(f): At 2Hz; ΔI=21.7425-21.735=0.0075mA; ΔV= 0.1379mV; R= 39V/W

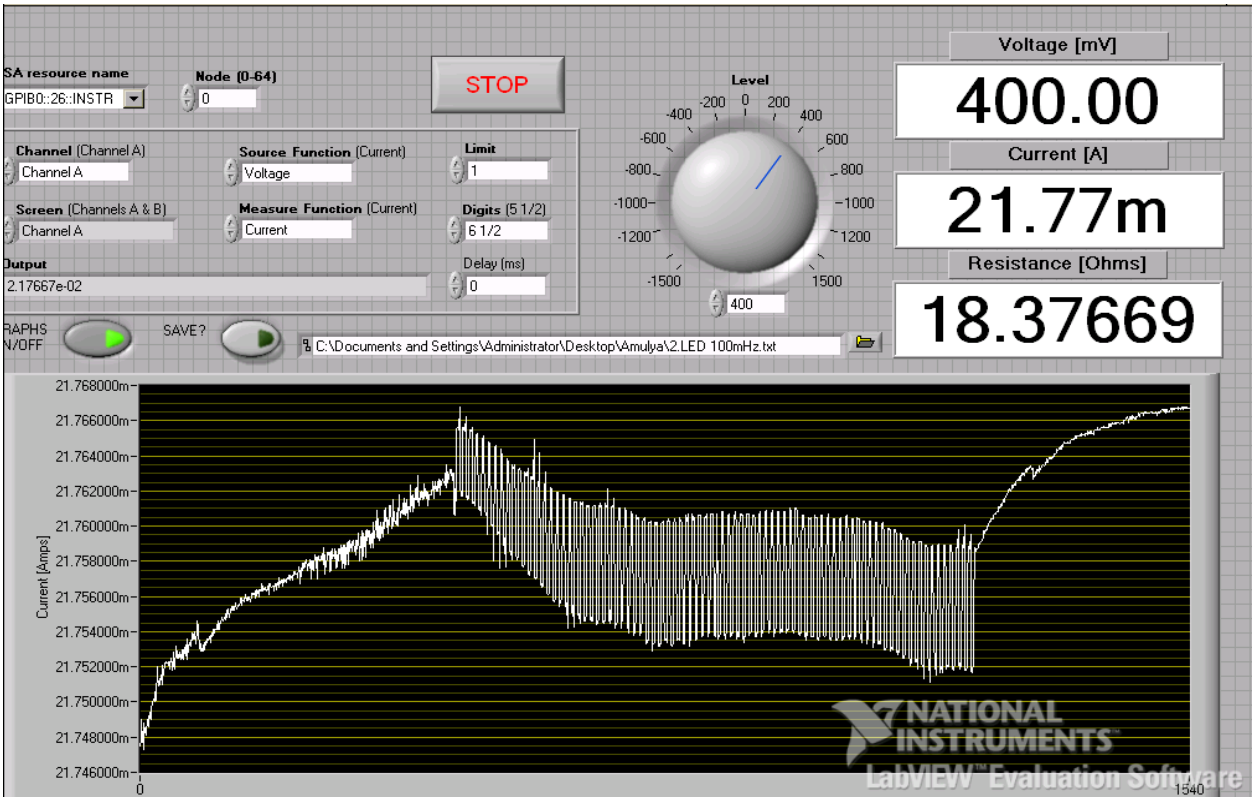

Figure 2.14(g): At 5Hz; ΔI = 21.761-21.754=0.007mA; ΔV= 0.1286mV; R= 36V/W

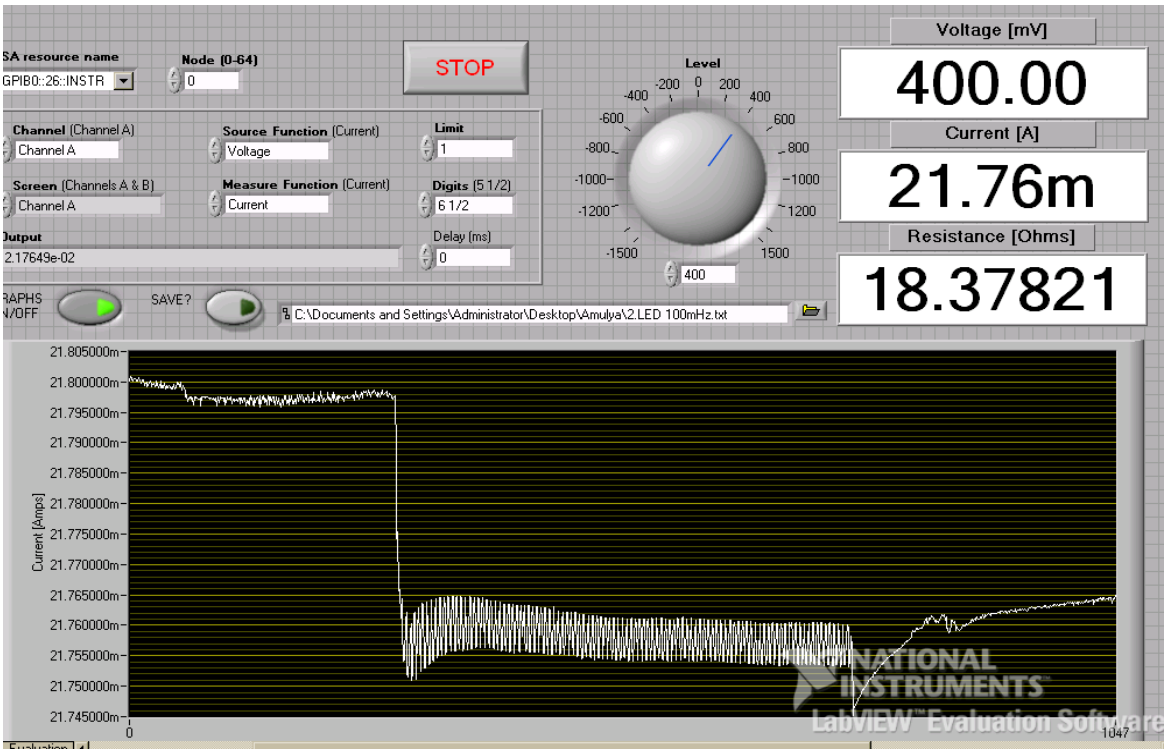

Figure 2.14(h): At 10Hz; ΔI=21.76-21.753=0.007mA; ΔV= 0.1286mV; R= 36V/W

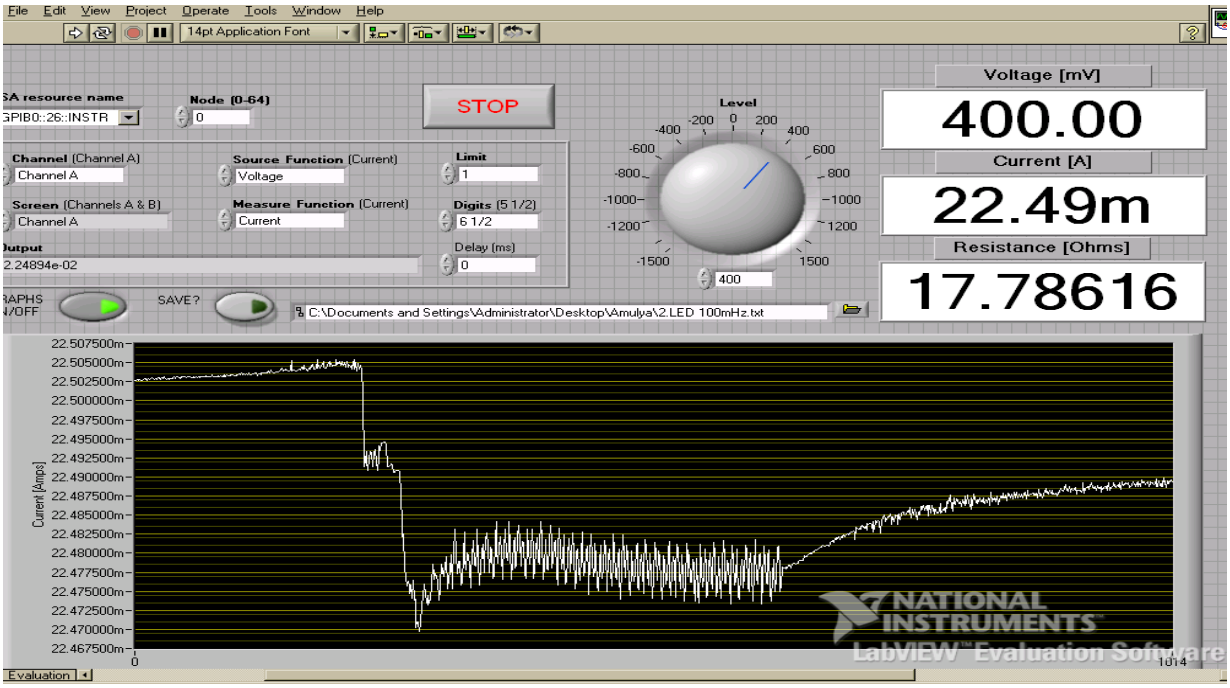

Figure 2.14(i): At 50 Hz; ΔI=22.4825-22.475=0.0075mA; ΔV= 0.1333mV; R= 37V/W

Figure 2.14: IR detection when modulated at the different frequency. (a) 50mHz (b) 100mHz (c) 200mHz (d) 500mHz (e) 1Hz (f) 2Hz (g) 5Hz (h) 10Hz (i) 50Hz.The display shows current versus time. 'R' represents the responsivity.

The Responsivity is even larger when we fabricated the device with Bow-tie and with the extended Bow-tie antennas as shown in the Appendix B.

From the above readings, the source is being modulated by connecting it to a Function generator. The LED source might have some delay to turn off/on completely when it is turned off/on. The Keithley also has some delay when detecting the signal. When the radiation is impinged on the Bolometer the heat may be dissipated to the substrate either through the contact pads and then to the substrate, or directly from the Bolometer to the substrate.

The Responsivity relation with change in modulation frequency is tabulated as follows.

Modulation frequency (Hz)	Responsivity (V/W)
0.05	206
0.1	140
0.2	50
0.5	41
1	41
2	39
5	36
10	36
50	37

Table 3.1: Responsivity vs modulation frequency

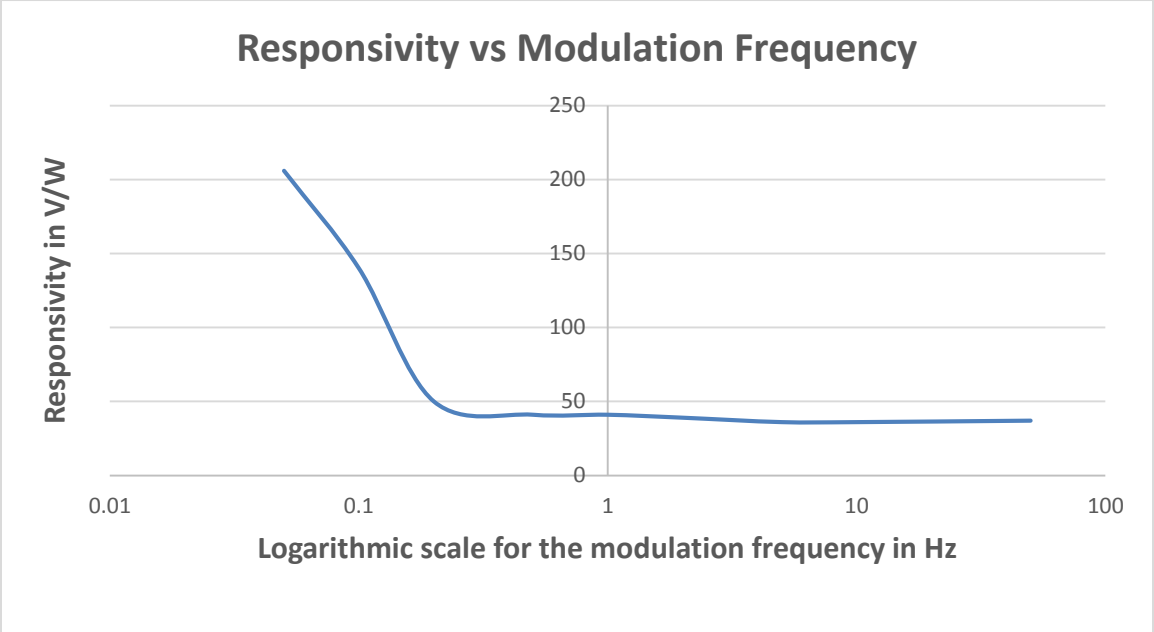

At low modulation frequency the responsivity is higher, presumably because the IR heats up the larger area, being absorbed by the Silicon, At frequencies above 0.2 Hz, S_V becomes independent of the modulation frequency. We will estimate the time constant and responsivity of the Pd bolometer from measured DC data below.

Palladium Bolometer:

The comparison of the Nb Bolometer and the Pd Bolometer DC characteristics are shown in Figure 2.15

As given in section 1.1, we re-quote the following equations,

$\beta = (\frac{1}{G_{th}})*(\frac{dR}{dT})$ and $\tau = \frac{C}{G_{th}}$; Therefore $G_{th} = \frac{1}{\beta}(\frac{dR}{dT})$

From $V = \frac{R_0}{1-\beta I^2} I$ [7] and $S_v = \beta * I_0$

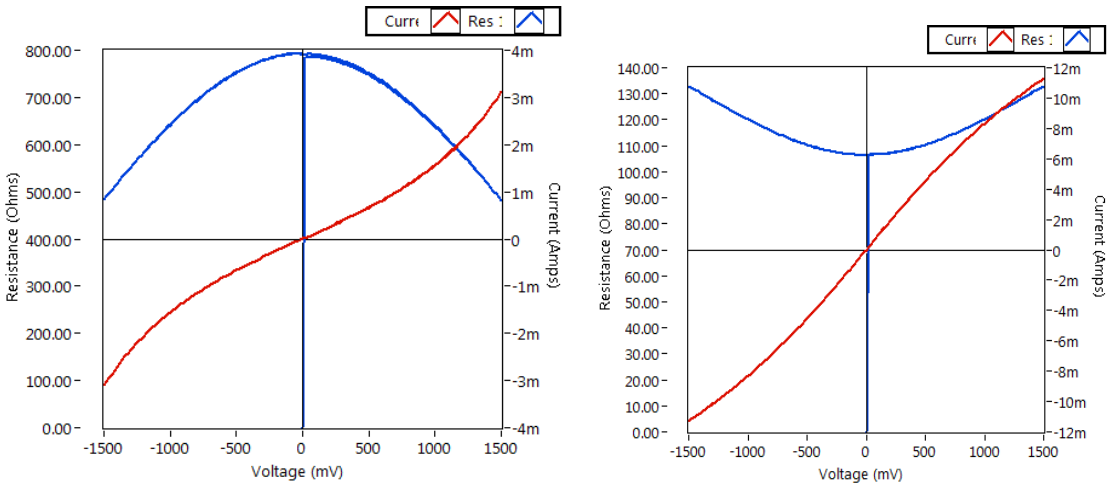

Figure 2.15: The comparison between Nb(left) and Pd(right) DC Characteristics

The β value for the Pd device has been found from the constant current biasing characteristic of the device and by curve fitting these values to equation (1.3) as shown in Figure 2.16.

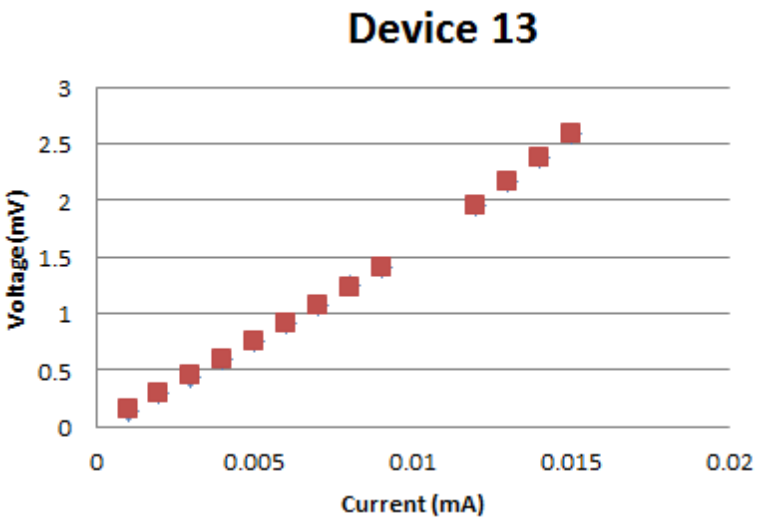

Figure 2.16: Curve fitting to find the value of β

From curve fitting β = 636 $\frac{V}{(W.mA)}$

The resistance with respective temperature property is measured by probing the gold contact pads on the device using 2 probe measuring equipment in the SIPL lab at

UMass, Amherst. The device is placed on the hot plate and the temperature measuring system is attached to the hot plate. Then the gold pads on the device is probed and the temperature of the hot plate is changed manually and the corresponding resistance values are noted using the Keithley 2600. The measured Resistance vs temperature for the 10µ Pd strip is as shown in Figure 2.17.

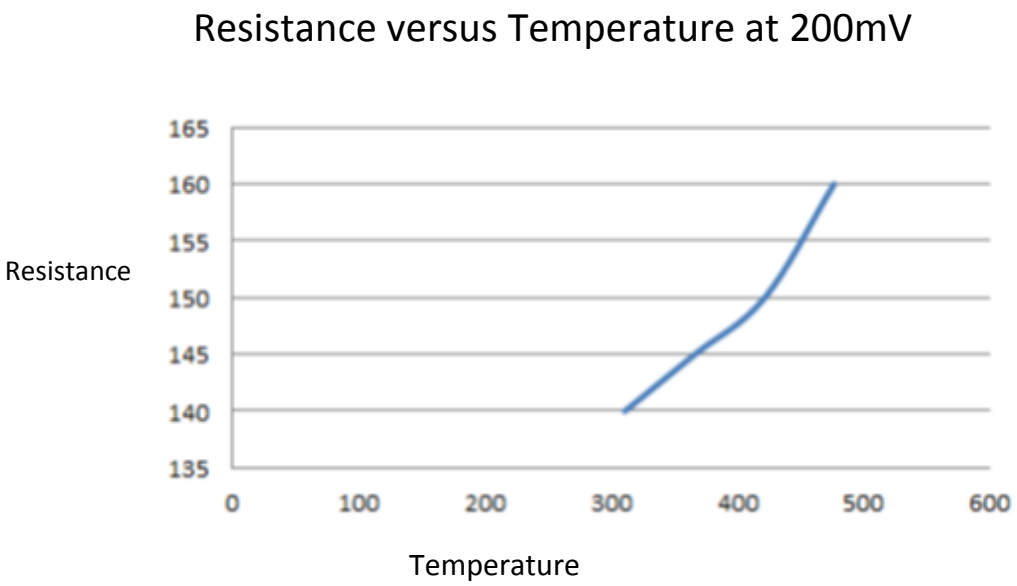

Figure 2.17: Variation of Resistance with Temperature for 10µ Pd strip

From figure 2.17, $\frac{dR}{dT} = \frac{160-140}{477.594-310.928} = 0.12\frac{\Omega}{K}$

Therefore from the Equation (1.14) $G_{th} = \frac{1}{\beta}\left(\frac{dR}{dT}\right) = \frac{0.12}{636} = 1.886 \times 10^{-4}\frac{W}{K}$

We know that $C = 1.87 * 10^{-13}\frac{J}{K}$; Therefore $\tau = 1.87 \times 10^{-13} / 1.886 \times 10^{-4} = 10^{-9}$ns = 1ns

The time constant we estimate is close to that estimated for a similar IR bolometer fabricated from Pt in [12]. The thermal conductance is also comparable to that of estimated in [12] if we assume that G_{th} scales with the device area. Based on this

"reality check" we believe that our estimate of the time constant is a good approximate value.

We can now also estimate $S_v = \beta * I_0 = 636 * 0.0217 = 13.8012 \frac{V}{W}$. This estimate of the responsivity is the "DC" responsivity since it has been derived from DC measurements of beta and I_0 and the responsivity we measured in table 3.1 is the optical responsivity.

CHAPTER 3

ROLL TO ROLL BASED CARBON NANOTUBES TERAHERTZ DETECTOR

3.1 Introduction

Carbon nanotubes based electronics promises greater flexibility compared to conventional silicon electronics as they can be fabricated on the flexible substrates. Besides being flexible devices the chance to make high volume manufacturing using the roll to roll nano manufacturing machine in polymer science department made me more interested in this project.

The carbon nanotubes based detector discussed in this thesis detects the THz radiation using the Bolometric principle. As explained in the section 1.1.3, the Bolometer changes its resistance and measures the power of the EM radiation as it heats up the bolometric material. When the DC power is supplied to the carbon nanotubes, it gives the initial energy to excite the elections in the bolometer. In the figure 1.2, carbon nanotubes act as an absorbing element.

3.2 Carbon nanotubes basics

Carbon nanotubes are cylindrical in shape. They can be thought of as rolled up sheets of Graphene, which is a single atom layer thick hexagonally connected Sp^2 bonded carbon atom sheet (Honey comb shaped).Carbon nanotubes can be either single walled or multi walled. Single walled carbon nanotubes can be thought of as single tubes, whereas multi walled carbon nanotubes can be thought of as a multiple

rolled layers (concentric tubes) of graphene as shown in the figure 3.1(a). Through rolling angle and the radius of the tubes we can determine the properties of the CNT's. $\vec{a}_1$ and $\vec{a}_2$ shown in the figure 3.1b are the unit vectors which define the basis in the graphene lattice structure. The chiral vector C, shown in equation (3.1) describes the circumference and the direction in which the nanotube has been rolled. The indexes n and m define the different combinations along the many directions upon which the CNTs can be wrapped as shown in the figure 3.1b [16].

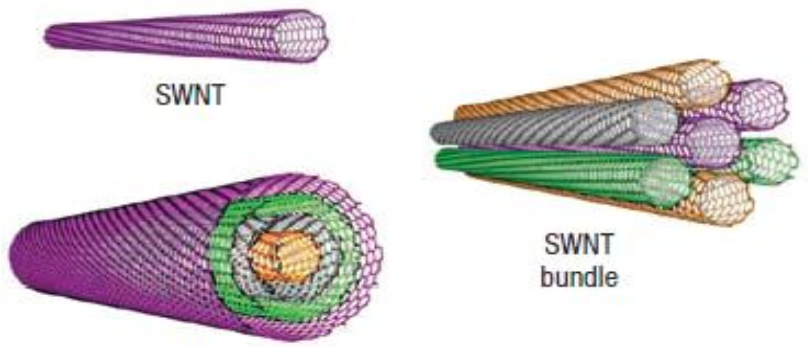

Figure 3.1a Carbon nanotubes structure [27]

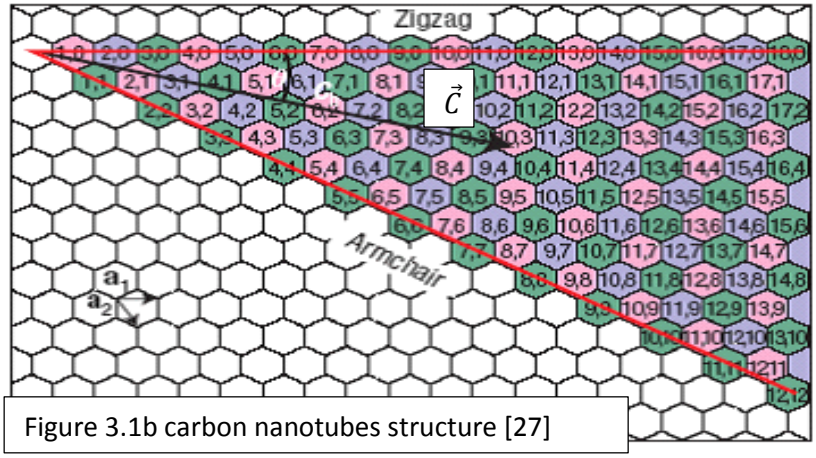

Figure 3.1b carbon nanotubes structure [27]

(3.1) $\vec{C}$= n$\vec{a}_1$+m$\vec{a}_2$

3.2.1 Electronic properties

The electrical properties of carbon nanotubes depend on how the hexagons are orientated along the axis of the tube [28]. So the electrical properties depend on n, m and the diameter of the tubes. If n=m (armchair tubes), the tubes have properties similar to that of metals i.e when you apply a voltage between two ends of an armchair nanotube, a current will flow. An armchair carbon nanotube is considered to be a better conductor than the copper normally used in electrical wire, or any other metal [28]. Even when $n \neq m$, and n-m = 3j, where j=1,2,3 …, the tubes have properties similar to metals. But when $n-m \neq 3j$, the tubes have properties similar to semiconductors. Semiconductor carbon nanotubes have energy gaps and will only conduct an electric current when extra energy in the form of heat, light or an electric field is applied to free electrons from the carbon atoms [29]. The CNT structure is Armchair structure if n, n; θ= 30; Zig zag structure for n,0; θ= 0 and Chiral structure if n,m for 0<θ<30

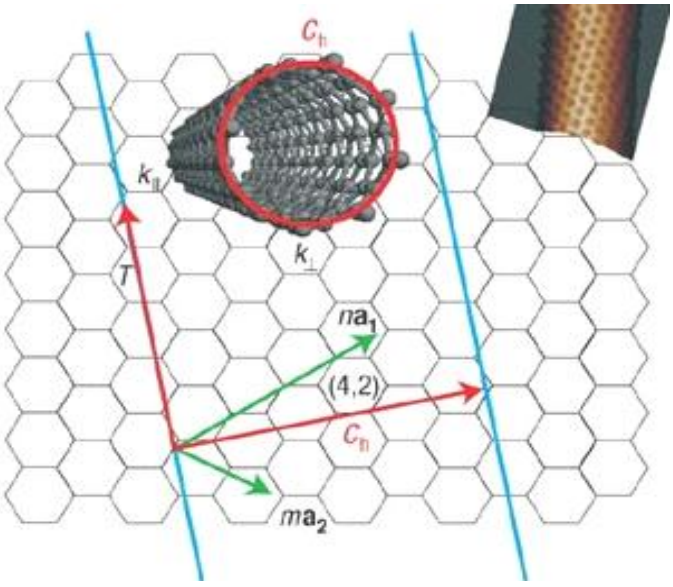

Figure 3.2: Graphene sheet indicating hexagonally connected carbon atoms. It also indicating chiral vectors [29]

The electrical resistance of the Carbon nanotubes significantly changes when other molecules gets attached to the carbon atoms [30]. This property can be used to develop sensors that can detect chemical vapors such as carbon monoxide [30].It has also been found that for all metallic nanotubes, the Fermi energy intersects two bands of the one dimensional band structure corresponding to two modes of conduction (i.e., one with positive velocity and the other mode corresponding to oppositely moving electrons, with negative velocity)—Carbon nanotubes have kinetic inductance about a thousand times greater than their magnetic inductance, which has implications in the high frequency electronic properties of nanotubes [31].

3.2.2 DC characteristics of Carbon nanotubes

The electrical properties (resistance, capacitance and inductance) of the carbon nanotubes, like in any other structure, arise due to internal structure and the external contacts. But, as carbon nanotubes are one dimensional, their transport properties are different when compared to the three dimensional materials. For example, the mean free paths (mfp) of a nanotube are much longer than those of bulk semiconductors. For acoustical phonon scattering (AC), the mfp can be greater than 1µm at room temperature, while for optical phonons (OP) the mfp is about 15nm [32]

Though the mean free path of the electrons when scattered off the OP is so small, the scattering processes do not occur at low energies, which is supplied by the bias voltage [33]. When 160mV is applied across the CNT OP scattering effects begin to show up. DC characteristics show the scattering effects of the CNT device. For a perfect

contact situation the maximum amount of current that can go through a single SWCNT can be calculated to be about 25μA due to OP scattering [16].

Using the Landauer formulism [34] and considering the number of modes to be 2 plus two spin modes we can calculate the minimum DC resistance of a single CNT to be approximately $R_{CNT}=h/2e^2M = 6.45K$ [16], but the actual measured resistance for CNT based devices depends greatly on the quality of the contacts. Contacts add to the total measured DC resistance of the CNT from a few KΩ to hundreds of MΩ. Also the choices of metals with work functions closer to the Fermi level of carbon, such as palladium (Pd), have also been shown [26] to improve contacts.

When the electron moves from 3D, i.e the contacts, to 1D Carbon nanotubes, the excess kinetic energy gives rise to kinetic inductance L_k. Similarly the change in the potential due to change in the charge density gives rise to quantum capacitance C_Q.

3.2.3 AC characteristics of the carbon nanotubes

Compared to DC electrical properties of nanotubes, describing AC properties is challenging because it is difficult to make a generally accepted model for the high frequency transport inside nanotubes due to the complexity added from the nanotubes low dimensionalities. It has been documented that the Landauer picture breaks down in 1D [35]. Burke [36] has proposed a model, in which he considers interacting electrons, rather than non-interacting electrons inside the well-known Fermi gas. Burke and others [37][38] have suggested the presence of a different medium: The Luttinger-Tomonaga liquid [39][40]. In this case, electron-electron interactions become relevant and affect

transport; In his theory, Burke arrives to a model which describes a nanotube as four parallel connected transmission lines with the previously mentioned L_k and C_Q as shown in figure 3.3 below.

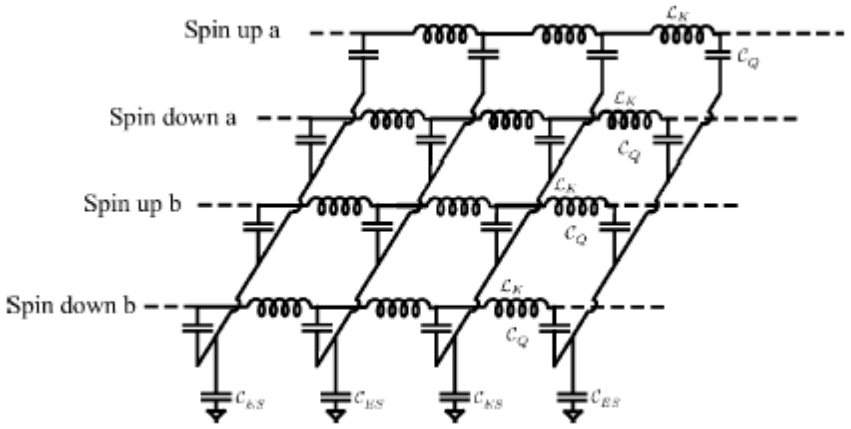

Figure 3.3 AC circuit model for interacting electrons. Four modes, 3 spin carrying, and 1 current carrying are coupled due to electron-electron interactions in a 1D conductor. From ref. [36].

A series resistance is added to the Transmission line to account for the nanotube DC resistance (R_{CNT}, as shown in the figure 3.4 below). Also L_K is divided by 4 and C_Q is multiplied by 4 as we have added the electrical effect of the four channels into one. Finally, we will add the effect of the contacts (contact resistance R_C and contact capacitance C_C) to the transmission line model as shown in figure 3.5.

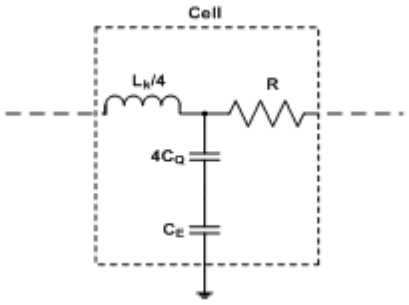

Figure 3.4: Unit cell of the transmission line model. It composed of a kinetic inductance, a quantum capacitance, a negligibly small electrostatic capacitance, and a series CNT resistance. Note: In this work we will denote R as RCNT [16]

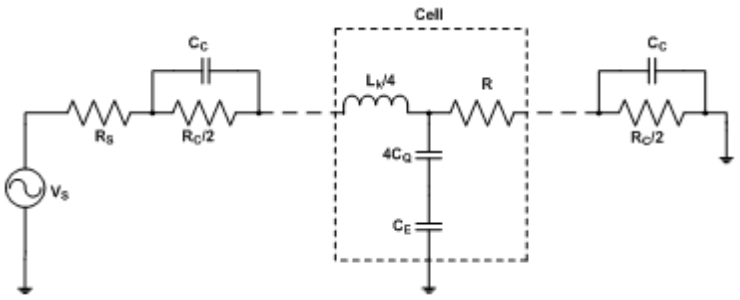

Figure 3.5: Modified Burke TL Model. Complete transmission line (TL) model used in this work to treat the CNT. Note that the complete model treats the CNT as a TL in series with the DC CNT resistance. Also, contact resistance (CR) and capacitance (CC) are added to the model device accurately [16]

3.3 Properties of the CNT networks/films

The detectors we have studied employ CNT networks, as versus the single tubes we have discussed so far. We will discuss networks of both SWCNTs and MWCNTs. The CNT networks are deposited by the roll to roll manufacturing.

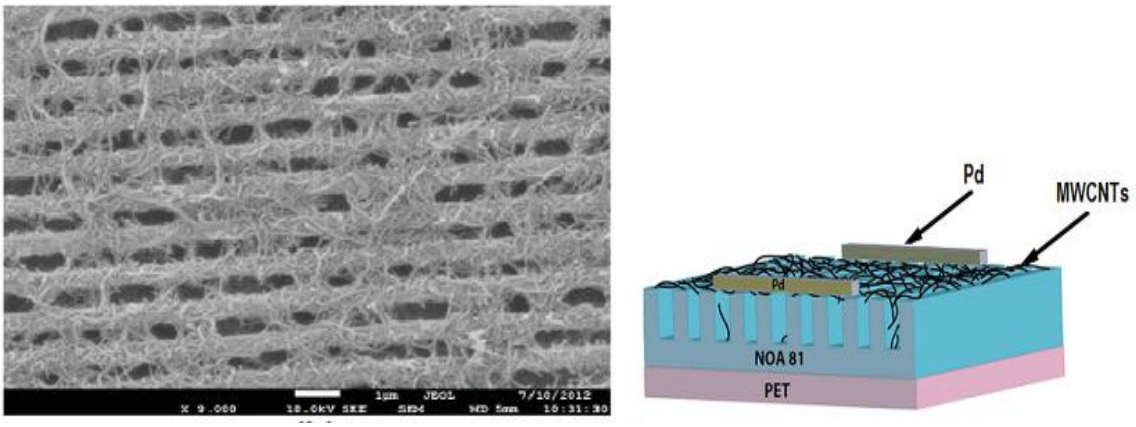

(a) **(b)**

Figure 3.6: (a) SEM image of suspended MWCNTs on PET substrate gratings [53]; (b) Schematic of a MWCNT-based infrared sensor [53]

As the dielectrophorosis process has not been employed, the carbon nanotubes deposited would include both metallic and semiconductor tubes. These tubes are suspended over the grooves to reduce the thermal link to the substrate. This enhances the enhanced bolometric performance using the roll to roll process.

The conduction through the network can be pictured statistically as shown in the figure 3.7

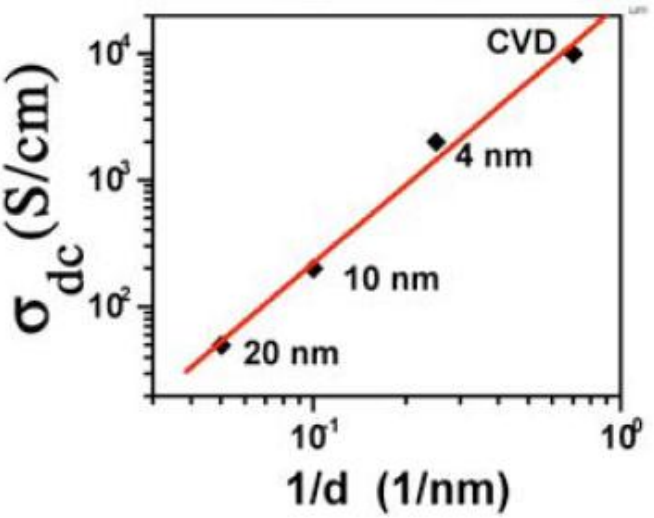

Figure 3.7: Network conductivity as a function of the nanotube bundle diameter, d [55]

In the figure 3.7 the conductivity is displayed as a function of the inverse of the bundle diameter. From the figure it can be observed that the smaller bundle size has larger conductivity. This is because the current flows at the surface of the bundles and the nanotubes in the interior do not contribute to the conduction process [55].

There are many contributions for the carbon nanotubes network resistance. The main contribution for any carbon nanotube device is the contact resistance. In case of

the network of the carbon nanotubes, the resistance is contributed due to many combinations of the metallic and semiconductor devices as shown below in figure 3.8

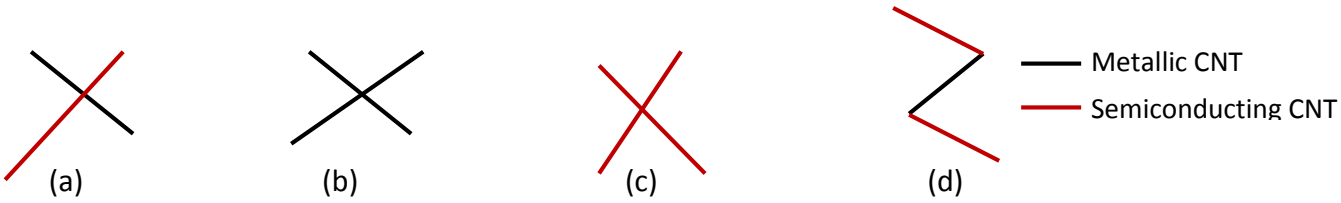

Figure 3.8: Different combinations of the CNT's in the CNT network. (a) Shows the contact resistance between metallic and semiconducting CNTs (b) shows the contact resistance between two metallic CNTs (c) shows the contact resistance between two semiconducting CNTs and (d) shows the contact resistance due to metallic, semiconducting and metallic CNTs

Theoretically, in the CNT films as the temperature is increased the contact resistance decreases due the fact that the electrons have greater average energy and can thus get over the barrier more easily. An Annealing process is usually done after the CNT fabrication process to reduce the contact barrier [58]. Note that we expect dR/dT to therefore be negative, whereas for Pd bolometers it is positive.

3.4 Device description and fabrication process

As mentioned in the section 1.2.3, the bolometer detects THz radiation. When the incident THz radiation heats up the CNT network, a measurable change in the CNT resistance is observed. The dependence of the electrical resistance on the temperature along with the low density, high surface area and negligible heat capacity of CNT's make them very responsive as they are sensitive to the incident THz radiation [53].CNT based bolometers can be broadly categorized into the following two groups

1. SWCNT-polymer composite films where SWCNTs are uniformly embedded in a polymer matrix [41-45].

2. Suspended SWCNT/MWCNT networks or individual bundles prepared by chemical vapor deposition (CVD) or vacuum filtration transfer [46-51]

Suspended Carbon nanotubes in air or in vacuum have been shown to reduce the thermal link to the environment and hence have a superior bolometric response [46-51]. For example, SWCNT/MWCNT network films were suspended in vacuum between supporting structures or electrodes that were a few millimeters apart and a dramatic increase in the photo response was observed at low temperature with a temperature coefficient of resistance (TCR) of ≈1% K^{-1} [46]. Lu and the coworkers in paper [48 and 49] reported an enhanced bolometric response when they are suspended on SiO2/Si substrates which were lithographically patterned with grooves. To fabricate the CNT's on the Si devices we have to use lot of time consuming processes like Ebeam lithography, CVD etc. Making a CNT device using these processes for high volume manufacturing Si devices might not be an efficient method. The roll to roll process mentioned in this section makes it easy for high volume manufacturing and is very efficient.

Our desire is to create a sensitive CNT based sensor on a flexible substrate that utilizes a suspended layer of carbon nanotubes on a submicron polymer grating. The expertise of Prof. Ken Carter and his Post doc Jacob John (of Polymer science department at UMASS, Amherst) in roll to roll (R2R) nano-imprint lithography enabled the replication of high resolution nanoscale patterns. More over the roll to roll machine has high throughput compared to the conventional silicon fabricated techniques like

Ebeam lithography and photolithography. The R2R process is a low cost, high speed and large volume technique to manufacture carbon nanotube based bolometer.

With the help of Jacob John (Postdoctoral student under Professor Ken Carter at Polymer science department at UMass, Amherst), we were able to design and fabricate a CNT based THz sensor on a flexible substrate.

The device fabrication process and detailed explanation of the Roll to Roll machine were given in the papers reference at [53] [54]. In this thesis I would give a brief overview of the device fabrication process. Figure 3.9 below gives an over view of the roll to roll terahertz bolometer fabrication process.

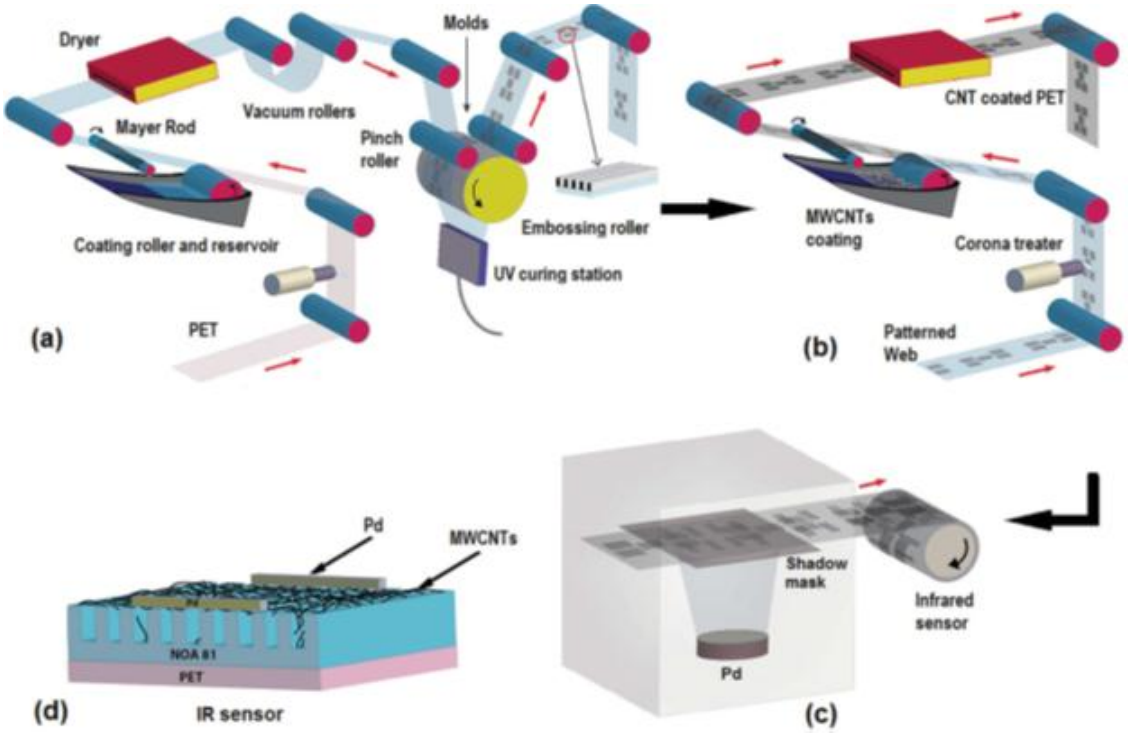

Figure 3.9: R2R processes for the fabrication of THz sensors: a) R2R coating and nanoimprinting, b) R2R deposition of MWCNTs, c) deposition of electrodes, and d) schematic of a MWCNT-based Near IR sensor [53].

The device is made on a PET (Polyethylene terephthalate) substrate. As shown in the (a) of the figure 3.9, first, a thin layer of of polyvinylpyrrolidone (PVP) was coated on the polyethylene terephthalate (PET) substrate to improve photoresist adhesion on PET [53]. A commercially available fast curing photocurable resin, Norland optical adhesive 81 (NOA 81) was used as the imprint resist material in the present work [53]. Now 35 wt % solution of NOA 81 in propylene glycol monomethyl ether acetate (PGMEA) is transferred to the PET substrate and the Mayer rod removes the excess resist material from the substrate. After the coating the solvent is dried at the drying station as shown in the (a) of the figure 3.9 above.

The PFPE (Perfluoropolyether) hybrid molds on the double sided adhesive tape is attached to a rubber cushion layer wrapped around the embossing roller. The molds contain grating patterns with line width of 500nm and of height 500nm with the same channel spacing. These gratings are continuously imprinted on to the resist coated on the PET substrate in the embossing section. The resist was immediately cured by the UV light at the UV curing station. The solidified nano features were continuously peeled off from the embossing roller/R2R mold assembly. The PET sheet coming out of the embossing roll is resent to the Roll to roll machine and the same process is repeated, but in place of the resist, carbon nanotubes are being coated as shown in the figure (b) of the figure 3.9 above

Then Palladium electrodes are sputtered using a shadow mask as shown in the (c) of the figure 3.9 above. The figure 3.9 (d) above shows the schematic of the Roll to Roll based CNT near IR detector. In the case of the NIR detector an LED source was

employed, similar to how we described NIR detection experiments with our Pd detector. Later in this Chapter, we will illustrate how the detectors were coupled to the THz laser beam.

The SEM analysis, shown in the figure 3.10 below, shows a uniform deposition of the MWCNTs and the tubes are well suspended on the trenches. In this research work we have worked on both SWCNTs and MWCNTs. We were not able to suspend SWCNTs on the trenches as they are more flexible compared to the MWCNTs.

The thickness of the CNTs can be varied by either varying the concentration of the solution or by varying the speed ratio of the coating roller or by using a different Mayer rod.

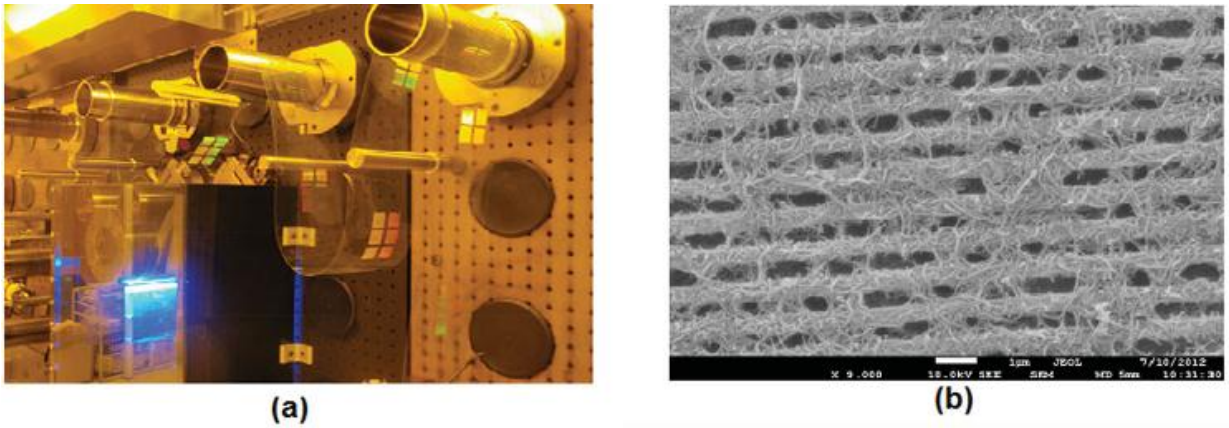

Figure 3.10: a) R2R NIL in process showing several meters of nanoimprinted PET substrate, b) SEM image of suspended MWCNTs on gratings [53]

The picture 3.11 below shows the optical image of the device with different sizes.

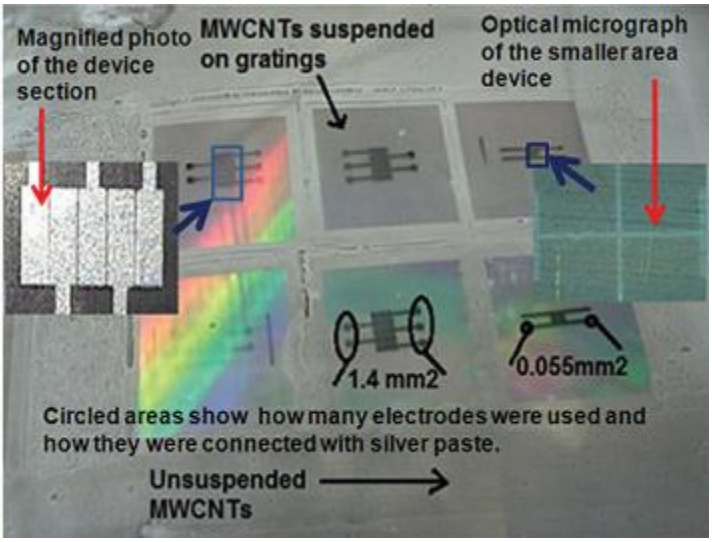

Figure 3.11: Photograph of the R2R fabricated devices showing electrodes. It is used for measurements

3.5 Results and discussion:

The experimental procedure for testing the Roll to Roll THz bolometer is similar to that we used for testing the palladium THz bolometer, explained in the section 2.5. The device is placed at the output of the THz laser and the THz radiation is modulated manually (as the device is too slow to use the modulator) by blocking and unblocking the input to the FIR laser using wood. The electrodes showed in the figure 3.11 above are connected to the Keithley 2600 using the probes and the electrical properties of the devices as tested when the modulated THz radiation is impinged on the device.

As the device is big in size compared to the Palladium bolometer explained in the section 2, there is no need to have lens or antenna to focus the radiation on to the device. I have worked with both Single walled carbon nanotubes and multi walled carbon nanotubes in this thesis work. As referenced in papers [46-51], the suspended tubes showed a better bolometric properties for near IR radiation compared to the

unsuspended tubes. In the Roll to Roll process we were not able to suspend the SWCNTs in between the groves (this might be because SWCNTs are more fragile compared to MWCNTs [56]). However the SWCNTs are fabricated and tested for the THz measurements as explained below.

3.5.1 SWCNT THz detection results for 1.2mm^2 device active area

The thickness of the SWCNTs films obtained range from 80nm to 110nm. The device is biased at different voltages and the change in current/resistance when the THz laser is modulated is noted. When the experiments were conducted the THz laser source has a power at the output as 1.3mW and the frequency was 1.9THz. The gap for the device with active area 1.2mm^2 is 100µm and the length is 12mm. The active area (bolometric area) for this device is 1.2mm^2. We can approximate the device area to be circular with the radius 'a'. Therefore

$$\Pi a^2 = 1.2 \longrightarrow a = 0.618\text{mm}$$

From equation 2.26 in [17], Power transmitted through a circular aperture near the axis with radius a is given by

$$P_{THz} = \frac{2 * Plaser}{\pi w^2} \int_0^a 2\pi r e^{\frac{-2r^2}{w^2}} dr = (1 - e^{\frac{-2a^2}{w^2}}) * P_{laser} \quad (3.2)$$

We can calculate transmitted power to the device (P_{Thz}) as $P_{laser} * (1 - e^{\frac{-2a^2}{w^2}})$

'w' is 6.45mm (see (a) in appendix A); 'a'= 0.618mm. These calculations assume that the laser beam is Gaussian, as was verified in [17]. Therefore power transmitted to the bolometer = 1.3*0.01819mW = 0.02365mW

(a)

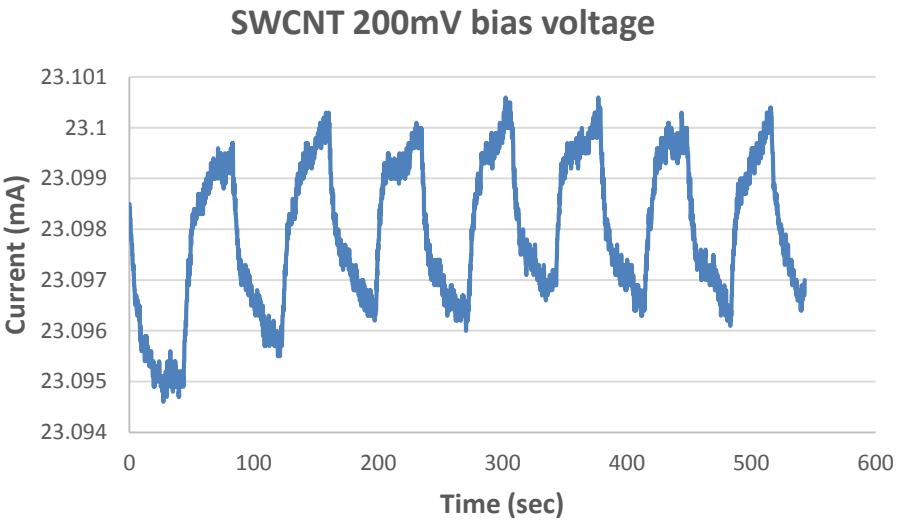

Figure 3.12 (a): SWCNT detection measurement. When the bias voltage is 200mV, ΔI = 23.1-23.095 = 0.005mA; R= 8.66 ohms therefore ΔV=0.0433mV. Responsivity = $\frac{\Delta V}{P_{THz}}$ = 0.0433mV/0.02365mW = $1.83086\ \frac{V}{W}$

(b)

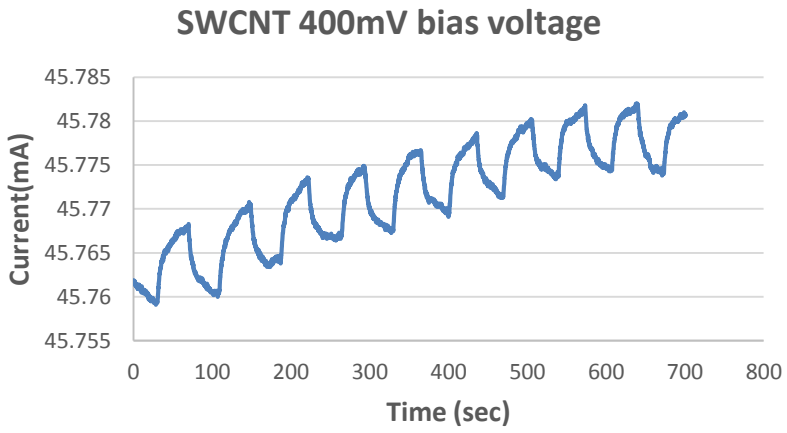

Figure 3.12(b): SWCNT detection measurement. When the bias voltage is 400mV, ΔI = 45.7698-45.7599=0.0099mA; R= 8.75 ohms therefore ΔV=0.086625mV; Responsivity = $\frac{\Delta V}{P_{THz}}$ = 0.086625mV/0.02365mW = $3.6625\frac{V}{W}$

(c)

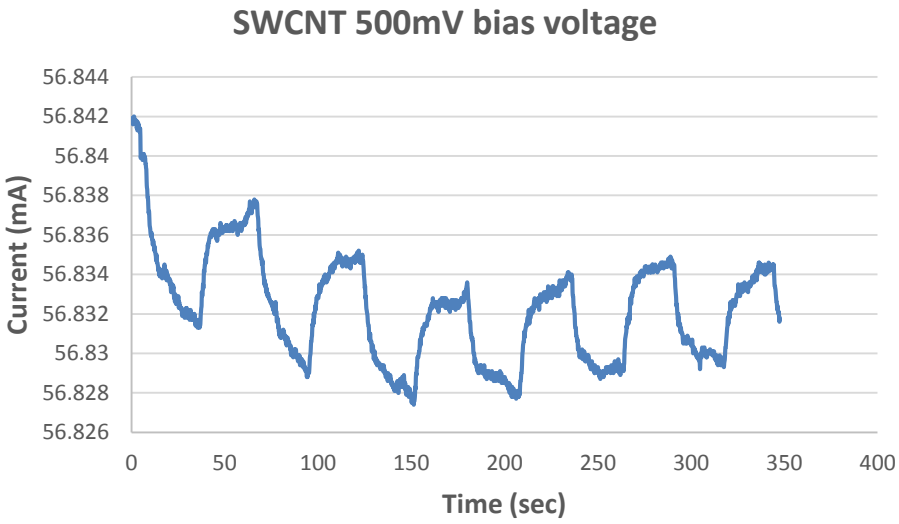

Figure 3.12(c): SWCNT detection measurement. When the bias voltage is 500mV, ΔI = 56.8375-56.8287= 0.0088mA; R= 8.8 ohms therefore ΔV= 0.07744mV; Responsivity = $\frac{\Delta V}{P_{THz}}$ = 0.07744mV/0.02365mW = 3.2744 $\frac{V}{W}$

3.5.2 MWCNTs detection measurements for 1.2mm^2 device active area:

As mentioned in the section 3.2, the suspended devices have better Bolometric properties compared to the unsuspended devices. We have worked on both suspended and unsuspended devices. The unsuspended devices do not have any grooves and they are coated on the resist instead of on the grooves in the unsuspended case.

3.5.2.1 THz detection measurements for the unsuspended and suspended MWCNT devices:

At 600mV (voltage at which we get minimum noise) bias voltage, the attempted detection by the unsuspended device is as shown below. Clearly, there was no detection above the noise level.

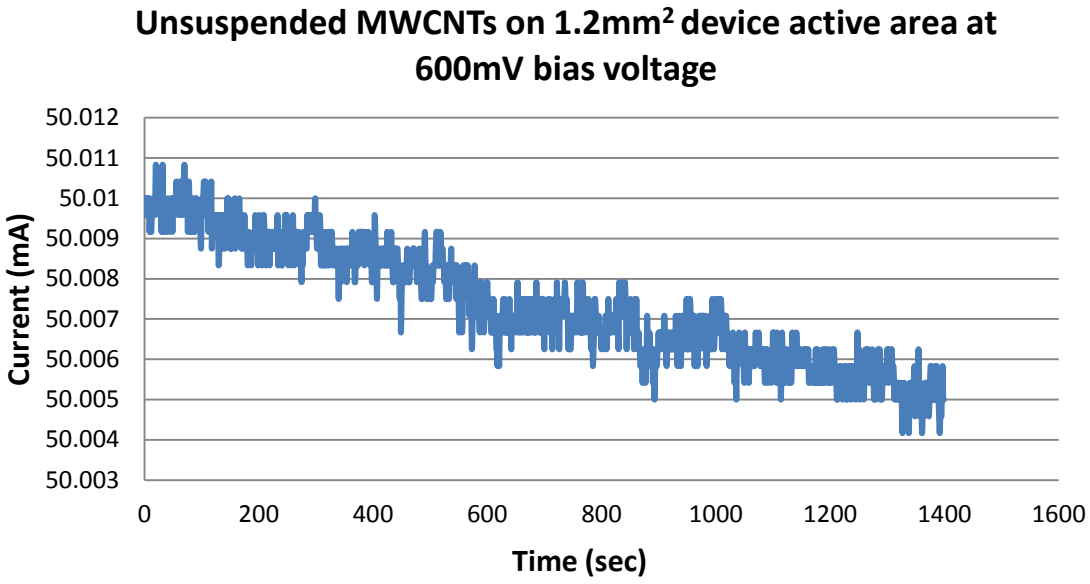

Figure 3.13 (a): Unsuspended MWCNT device THz detection. The signal is predominantly noise

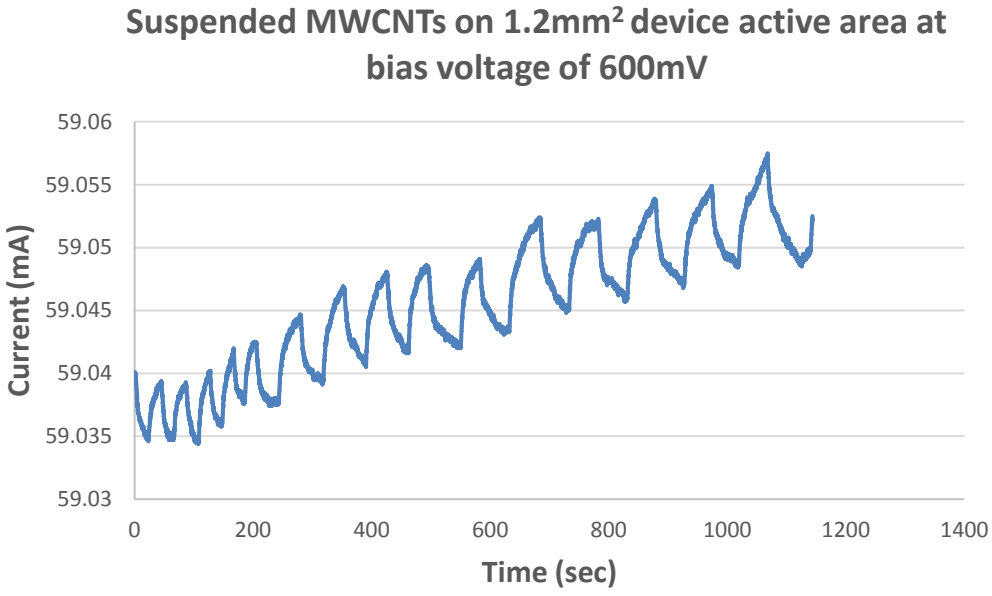

Figure 3.13 (b): Suspended MWCNT device THz detection

When the bias voltage is 600mV, ΔI = 59.0521-59.0432= 0.0089mA; R= 10.17 ohms therefore ΔV=0.0905mV; Responsivity = $\frac{\Delta V}{P_{THz}}$ = 0.0905mV/0.02365mW =3.8266 $\frac{V}{W}$

Comparison between suspended and unsuspended devices:

A dramatic increase in the bolometric response can be achieved when the thermal link of the carbon nanotubes with the substrate is minimized by suspending the tubes across the grating. The naturally suspended inner CNT shells in multiwall tubes provided an ideal configuration to enhance the bolometric effect by improving THz absorption and by reducing the thermal link [53]. This feature makes the MWCNTs better bolometric element compared to SWCNT [57].

3.5.3 The MWCNTs detection measurements of a device with active area of 0.055mm^2

The gap between the electrodes for the device with active area of 0.055mm^2 is 50µm and the length is 1.1mm.We re-calculate the power for the smaller devices area to be 0.001093 mW. From equation 2.26 in [17]

$P_{THz}$for 0.055mm^2 device = P_{laser}* $(1 - e^{\frac{-2a^2}{w^2}})$, where 'w' is 6.45mm (see (a) in appendix A)

$\Pi a^2 = 0.055$, there a = 0.1323mm and P_{THz} = 1.3 *0.00084109= 0.0010934mW

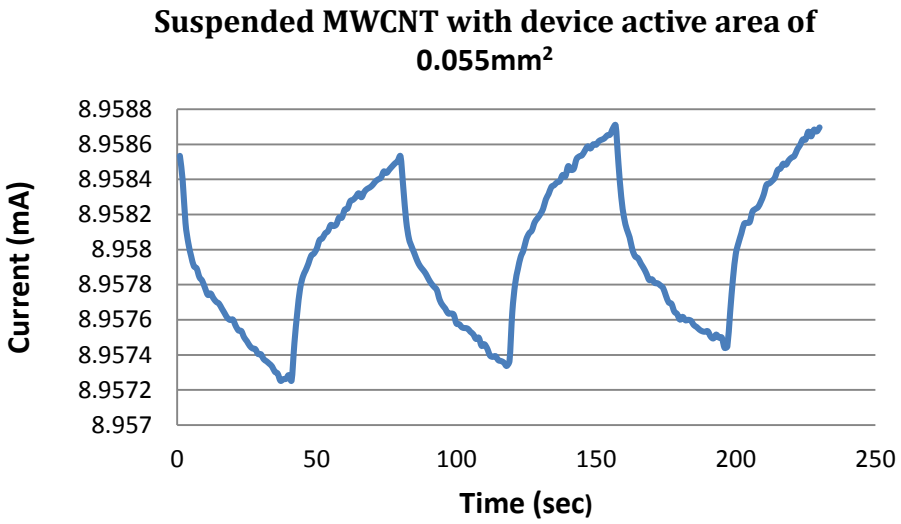

Figure 3.14: Suspended MWCNT with device active area of 0.0055mm²

At 600mV bias voltage, ΔI = 8.9587-8.9573 = 0.0014mA; ΔV = 0.0014*66.98=0.09377mV

Responsivity = $\frac{\Delta V}{P_{THz}}$ = 0.09377/0.001093 = 85.79 V/W;

Comparison between MWCNTs of 1.2mm² active area and 0.055mm² active area:

The Responsivity of MWCNT with 1.2mm² active area = 3.8266 $\frac{V}{W}$

The Responsivity of MWCNT with 0.055mm² active area = 85.79 V/W

So we observed that the responsivity increased significantly with the decrease in the active area. We will return to this comparison at the end of this chapter.

3.5.3.1 The THz detection of MWCNT device with active area of 0.055mm² at different bias voltages

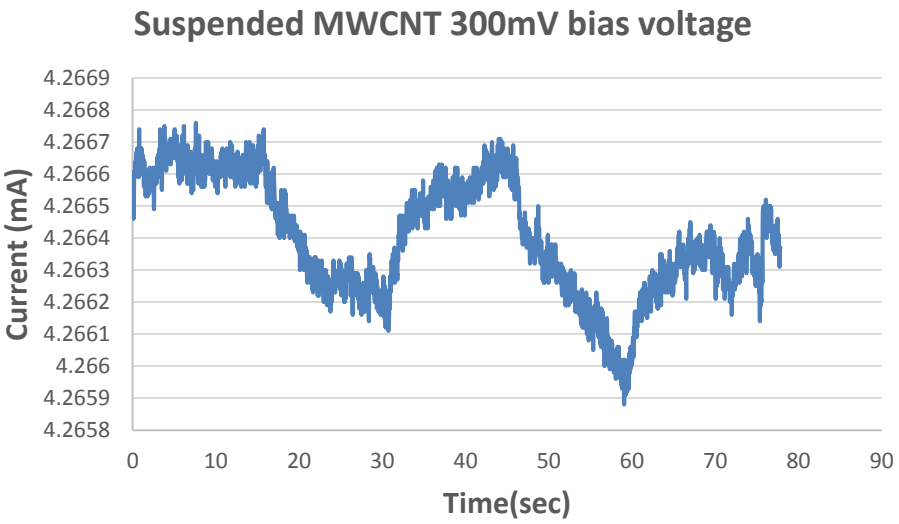

Figure 3.15 (a): Suspended MWCNT device detection at 300mV bias voltage

ΔI = 4.2666-4.2658 = 0.0008; ΔV = 0.0008*70.32 = 0.0562; Responsivity = 0.0562/0.001093 = 51.469 V/W

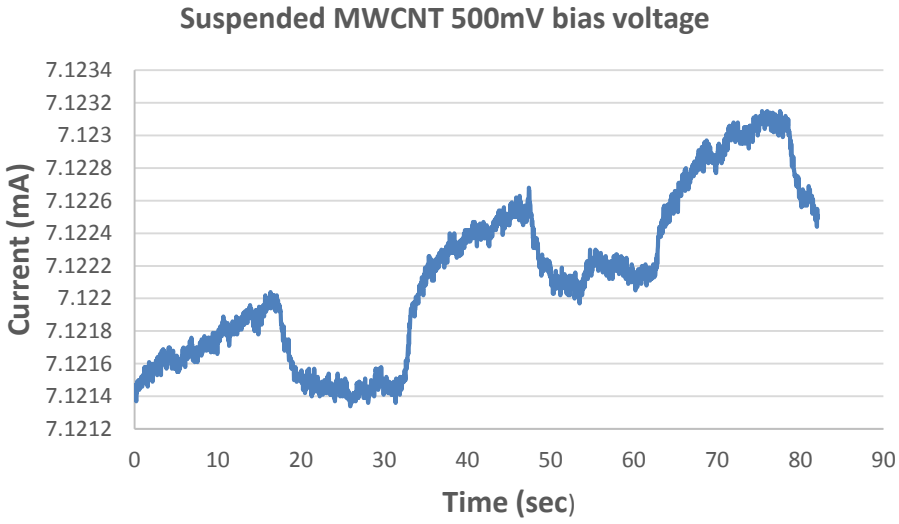

Figure 3.15 (b) Suspended MWCNT detection at 500mV bias voltage

ΔI = 7.1225-7.1214 = 0.0011mA; ΔV = 0.0011 *70.22 = 0.07724mV; Responsivity = 0.07724/0.001093 = 70.669 V/W

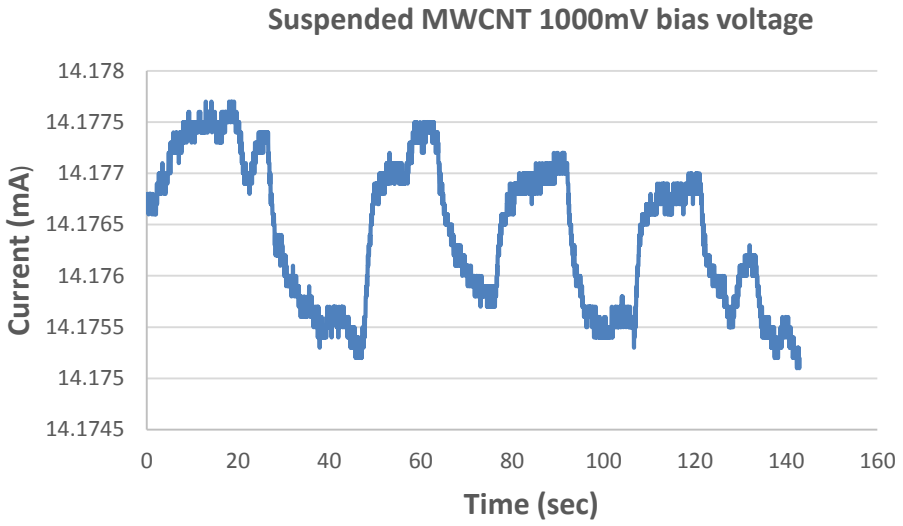

Figure 3.15 (c) Suspended MWCNT detection at 1000mV bias voltage

ΔI = 14.1775-14.1753= 0.0022mA; ΔV = 0.0022 *70.55 = 0.1552mV; Responsivity = 0.1552/0.001093 = 142V/W

Bias Voltage (mV)	Responsivity (V/W)
300	51.4
500	70.6
600	85.7
1000	142

Table 3.2 The Responsivity vs bias voltage of MWCNT devices with the smaller area

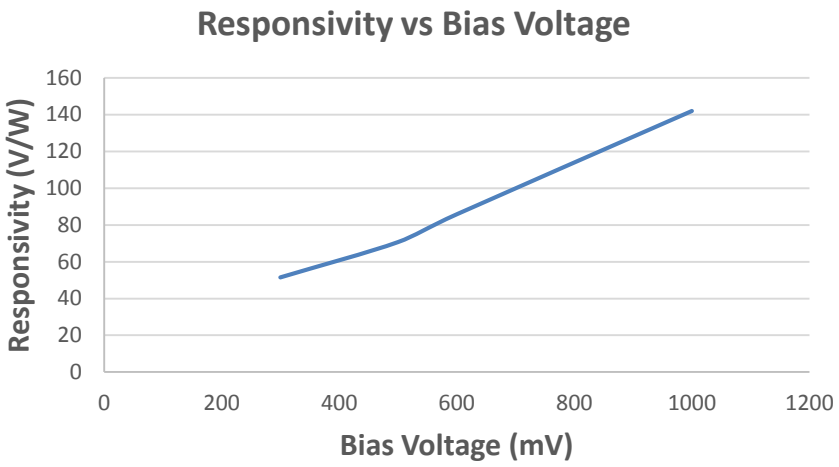

Figure 3.16: Relationship between bias voltage and responsivity of the MWCNT THz bolometer

We note that the responsivity is a linear function of the bias voltage, and thus also a linear function of the bias current, since the resistance barely changes. This behavior is expected for a bolometer as we showed in the equation 1.5 of the section 1.1.

3.6 Time constant (τ) calculation

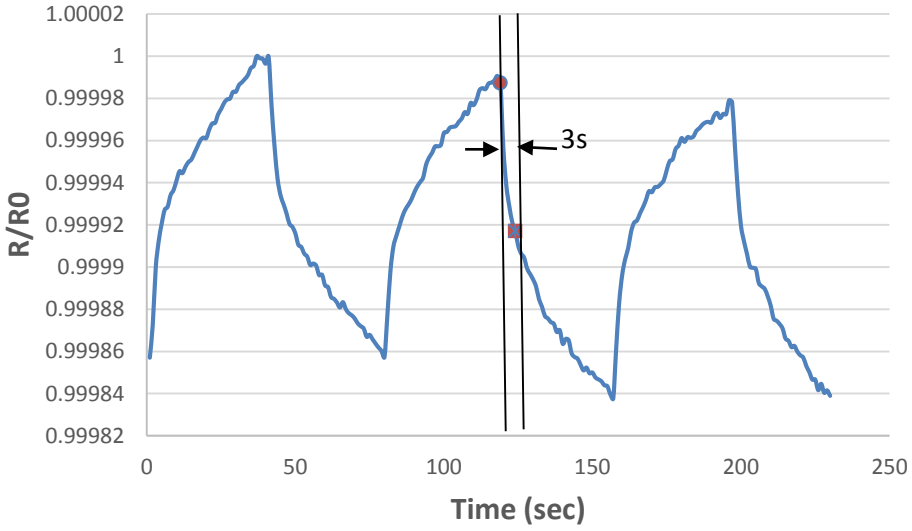

Figure 3.17: Response time measured at 50% magnitude change in signal for suspended THz detector of 0.055mm^2 active area on PET

As can be seen from the response above there are two parts. One with the fast time response and other much slower. The fast response may be due to the heat transfer from the MWCNTs to the resist/polymer, while the slow response may be due to the heat spreading further into the polymer.

As given in the equation 1.2, $\tau = \frac{C}{Gth}$, the time constant depends on the thermal conductivity of the substrate. The rise in temperature of the MWCNT films upon exposure to the THz radiation can be calculated using the relation of temperature coefficient of resistance (TCR). TCR is defined as the change in the resistance of the device when the temperature is changed by 1 Kelvin.

TCR = $\frac{1}{R}\frac{dR}{dT}$. From the experiments TCR is calculated as 0.08%/K. Therefore the rise in temperature of the MWCNT films upon exposure to the THz radiation is about 0.3K. As the MWCNTs are heated up, there is a 3 step process by which the energy is conducted to the environment [53].First, the hot electrons in the MWCNTs relax their energy to the phonons in the MWCNTs. The phonons then heat the resist and the PET substrate through interface phonon processes after which the heat is transferred to the environment.

We have assumed that the heat transfer is only from the MWCNTs to the substrate and not to the contacts. A detailed analysis for such heat transferred is performed for the SWCNTs [59] and the same process can be applied to the MWCNTs. Based on equation 1.2, by comparing the heat capacity of the SWCNT and MWCNT, it is

found that the time constant is 10^3 times larger. This limiting thermal conductance is likely to be from the phonons to the substrate.

The "bottle-neck" for transfer of heat from our devices must be from the substrate to the environment [53]. The thermal conductivity of the photoresist and the PET is much lower than that of inorganic substrates like silicon/SiO 2 on which CNT bolometric devices have usually been fabricated and this explains the somewhat longer time constants we measure [53]. By replacing the PET substrate with a higher thermally conductivity substrate, such as metal foil, the response time would be expected to decrease considerably [53].

3.7 Comparison between theoretical and measured responsivities:

Roll to Roll MWCNT bolometer with different active areas, discussed in the chapter 3 have similar $\frac{dR}{dT}$, therefore the theoretical responsivity of both the devices should depend on G_{th} and I_0.

From (1.4 &1.5) $\beta = (\frac{1}{G_{th}})*(\frac{dR}{dT})$ & $S_v = \beta I_0$

G_{th} is proportional to the device area. Therefore S_v is proportional to $\frac{I_0}{\text{Device area}}$.

I_0 for device with active area of 0.055mm^2 is 8.95mA and I_0 for the device with 1.2mm^2 area is 58.99mA. Therefore for

1. MWCNT with area 0.055mm^2, S_v is $(\frac{8.95mA}{0.055mm2})*\frac{dR}{dT}$ =162.7*10^{-6}(mA/ µm^2)* $\frac{dR}{dT}$

2. MWCNT with area of 1.2mm^2, S_v is $(\frac{58.99mA}{1.2mm2})*\frac{dR}{dT}$ =49.15*10^{-6} (mA/ µm^2)* $\frac{dR}{dT}$

As we measured the bolometer with 0.055mm^2 active area has better responsivity than the responsivity of bolometer with 1.2mm^2 active area.

Measured responsivity for 0.055mm^2 device area = 85.79 V/W

Measured responsivity for 1.2mm^2 device area = 3.8266 $\frac{V}{W}$

Based on the theoretical calculations in the

$$\frac{\text{Theoretical Responsivity of device with active area}0.055\text{mm}^2}{\text{Theoretical Responsivity of device with active area }1.2\text{mm}^2} = \frac{162.7}{49.15} \cong 3.3$$

$$\frac{\text{Measured Responsivity of device with active area}0.055\text{mm}^2}{\text{Measured Responsivity of device with active area }1.2\text{mm}^2} = \frac{85.79}{3.8266} \cong 23$$

CHAPTER 4

SUMMARY, CONCLUSION AND FUTURE WORK

4.1 Summary

The table summarizing the data of the Bolometer is shown below

Detector	Resistance (Ohms)	Area (mm^2)	S_v (V/W)	Bias Voltage & Bias current	G_{th} (W/K)	C (J/K)	Time constant (τ)	$\frac{1}{R}\frac{dR}{dT}$ (%/K)
Pd IR detector	19	$9x10^{-6}$	41	0.4 V & 21mA	$1.886x10^{-4}$	$1.87*10^{-13}$	1ns	0.06
MWCNT Large area detector	10.17	1.22	3.8	0.6 V & 5.9mA	Low	Large	10s	0.08
MWCNT small area detector	67	0.055	86	0.6V & 8.95mA	Low	Medium	3s	0.08
MWCNT small area detector	70.5	0.055	142	1V & 14.18mA	Low	Medium	4s	0.08

Table 4.1: Summary of Palladium IR bolometer and MWCNT Thz bolometer

4.2 Conclusion

4.2.1 Palladium Bolometer

Optical responsivity should be technically less than that of the DC responsivity. But as we observed in the 2.6.2.1, the optical responsivity is higher than the DC responsivity. The reasons why the optical responsivity is higher than the DC responsivity might be

(1) The LED illumination may be more concentrated than we assumed.

(2) The effective area of the bolometer may be larger than its physical area, which we assumed in calculating the optical responsivity. The bolometer is likely to act as a dipole antenna to some extent since it has dimensions close to the wavelength of the radiation, the rectangular pads may also contribute somewhat to the effective area.
(3) We note that ref. [12] estimated optical responsivities from 1,000 V/W (micron-size devices) to 30,000 V/W (a device of size 600 nm x 300 nm) for their Pt bolometers.
(4) Finally we note that only the responsivities we measure at modulation frequencies of 0.5 Hz or greater are independent of the modulation frequency and that the larger responsivities for slower modulation rates clearly show much longer time constants. We hypothesize that the slow detection process may be associated by the radiation being absorbed in the silicon substrate, and then indirectly heating the bolometer. Such a process would clearly involve a much larger heat capacity and thus be much slower. This process could also result in greater responsivity since the radiation would be absorbed over a much larger area. The fast process we observe, on the other hand, is very likely to be associated with the estimated time-constant of 1 ns.

4.2.2 Roll to Roll based carbon nanotubes THz detector

The measurements in section 3.7, overestimated the responsivity of the small area device compared with what we would expect based on the ratio of the areas and the currents. This may have happened if the effective area of the smaller device was actually larger than the physical area of the MWCNTs. An explanation for this would be that the contact pads of the smaller device acted as THz antennas, which would pick up a greater portion of the power in the incident laser beam.

A further contributing factor may be that the thermal conductance may not have scaled in the way we assumed. We note that the thermal conductance has two components: one represents conduction vertically into the substrate and is proportional to the area whereas the second component represents conduction horizontally to the contacts and is inversely proportional to the size of the gap. Thus the thermal contact resistance is somewhat more dominant in the device with small area (small gap ~50μm), which decreases the responsivity of the device compared to the device with larger area (as in the case of the device with the larger gap (100μm) the MWCNT resistance to the substrate is dominant compared to the contact resistance). The relatively larger thermal conductance per unit area would decrease the responsivity for the smaller device compared with that of the larger one. We therefore conclude that the first effect we discussed above (the antenna effect) must have dominated.

The thermal time constant of the device is given in the equation 1.2 as $\tau = \frac{C}{G_{th}}$, where C is the heat capacity of the MWCNT and the G_{th} is the thermal conductance. Here, C is proportional to the area of the MWCNTs, assuming that the thickness was the same for both devices. If Gth is due to heat conduction directly to the substrate, then the time constant would not depend on the device area. However, we measured that the time constant for the larger area device is larger (10s) than that of the smaller area device (3-4s). This gives us another indication that the heat conduction must have occurred to a greater extent through the contacts in the smaller device, as we discussed above.

4.3 Future work

4.3.1 Antenna design for the Palladium bolometer

The main resonance is determined by the antenna and it can be tuned by changing the antenna dimensions of interest. Based on the private communication with Martin Muthee of THz laboratory at UMass, Amherst, the double patch antenna radiates from the slot between the two patches. Therefore the slot should be designed to have the same length as given for the bow-tie antenna to detect Terahertz radiation. The antennas can be tested using simulations, before fabricating and testing the device. As the Palladium bolometer detects Infrared radiation, I believe that if we change the antenna design, we will be able to detect the Terahertz radiation. Jiayue of Physics department has used the antenna design I have with a narrower slot width (1µm) and he saw a Thz detection with Graphene bolometer.

4.3.2 Roll to roll CNT bolometer

The main drawback of the roll to roll based CNT detector is its slow detection. This is mainly due to the poor thermal conduction of PET. This can be improved either by adding gold nano particles in the resist or by incorporating a metal foil which can dissipate the heat quickly. This has already been tried and was successful in improving the time constant of the Infrared detection as shown in the figure 4.1.

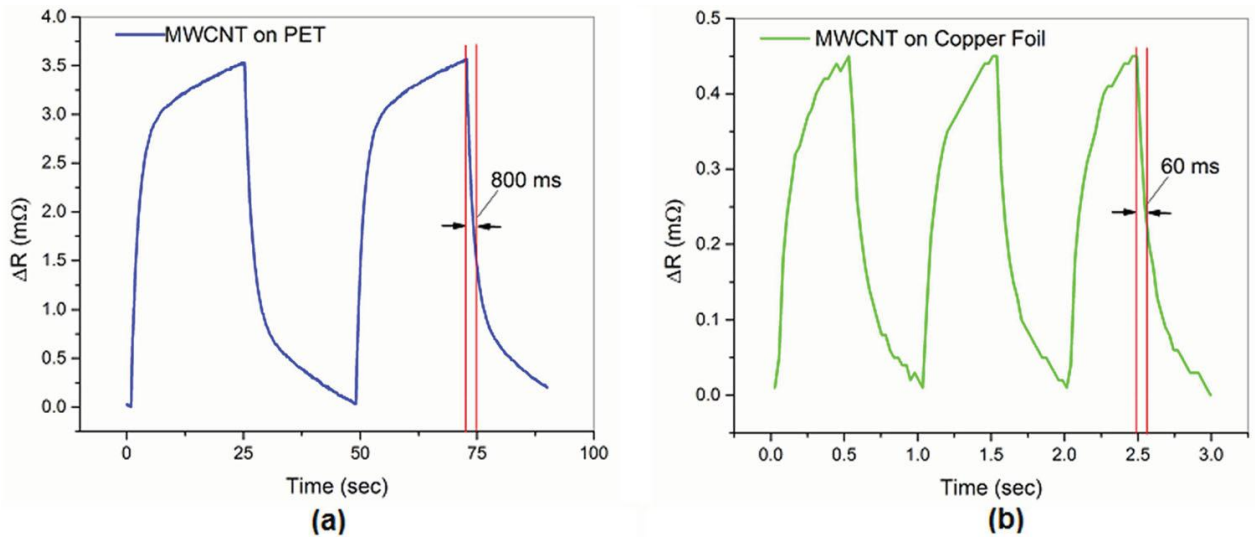

Figure 4.1: a) Response time measured at 50% magnitude change in signal for suspended IR sensor on PET(800ms) b) response time (60ms)for device on copper [53].

Incorporating an antenna in the design may also improve the responsivity of the device and my lab mates Martin Muthee and Jacob John are working on a new antenna design shown below.

Figure 4.2: Slot antenna design to improve the responsivity of the MWCNT bolometer (Martin Muthee and Jacob John are working on the design)

4.3.3 Terahertz integrated circuits

Terahertz integrated circuits is the ultimate goal of this project. The main idea behind the integrated circuits is to have a source and detector on the same circuit. The source will be the SWCNT based THz source [22] and the detector would be a CNT based on a Palladium based detector on silicon. The transmission between the source and the detector can be achieved through the transmission lines. This kind of integrated circuits will lead to the more sophisticated circuits that would work as "THz spectrometers on a chip".

APPENDIDIX A

THz BEAM DIAMETER (APPROX) AS MEASURED AT THz LABORATORY, UMASS, AMHERST

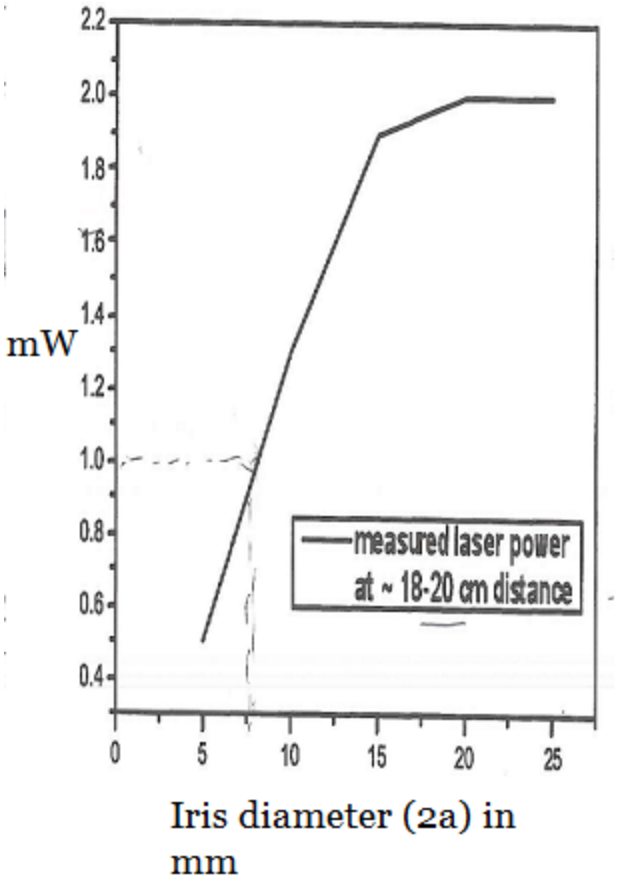

(a) From the [17] P within radius 'a' is given by 1-$e^{\frac{-2a^2}{w^2}}$;

At half power point $e^{\frac{-2a^2}{w^2}}$ = 0.5; Therefore w ≅ 1.7a; From the graph above

$2a_{1/2}$=7.6mm; Therefor w= 6.45mm

(b) In the case of the Infrared LED used to test the Palladium bolometer explained in the chapter 2, the power from the LED is down to ½ of maximum when the angle is about 5 degrees (based on the discussion with my lab mate, Martin Muthee), which is about 1/10th of a radian. The distance we estimated from the LED to the device is 1.5mm.Which makes the radius of the beam at that distance to be 0.1*1.5mm=0.15mm.

From the [17] P within radius 'a' is given by $1-e^{\frac{-2a^2}{w^2}}$;

At half power point $e^{\frac{-a^2}{w^2}} = 0.5$; $\frac{-a^2}{w^2} = -0.693$ which implies w=1.2a

Where 'a' is the radius of the beam at that distance which is 0.15mm.

Therefore w=0.18mm

APPENDIX B

INFRARED DETECTION DATA FOR THE PALLADIUM BOLOMETER WITH THE BOWTIE ANTENNAS

The performance for the device with Bowtie antenna can be calculated as

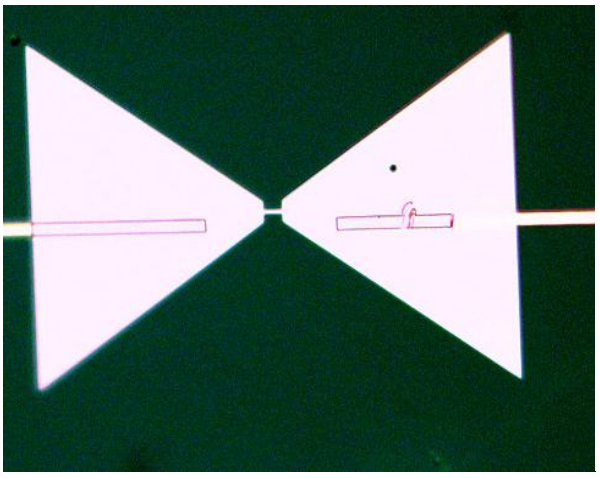

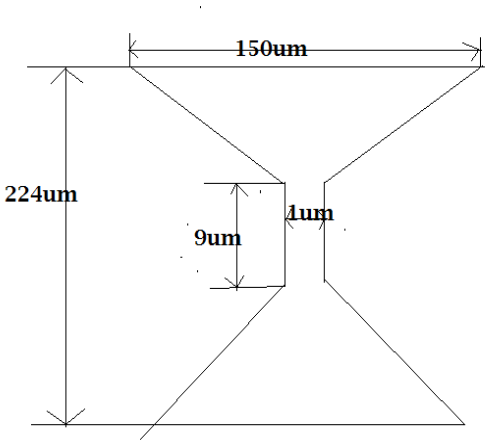

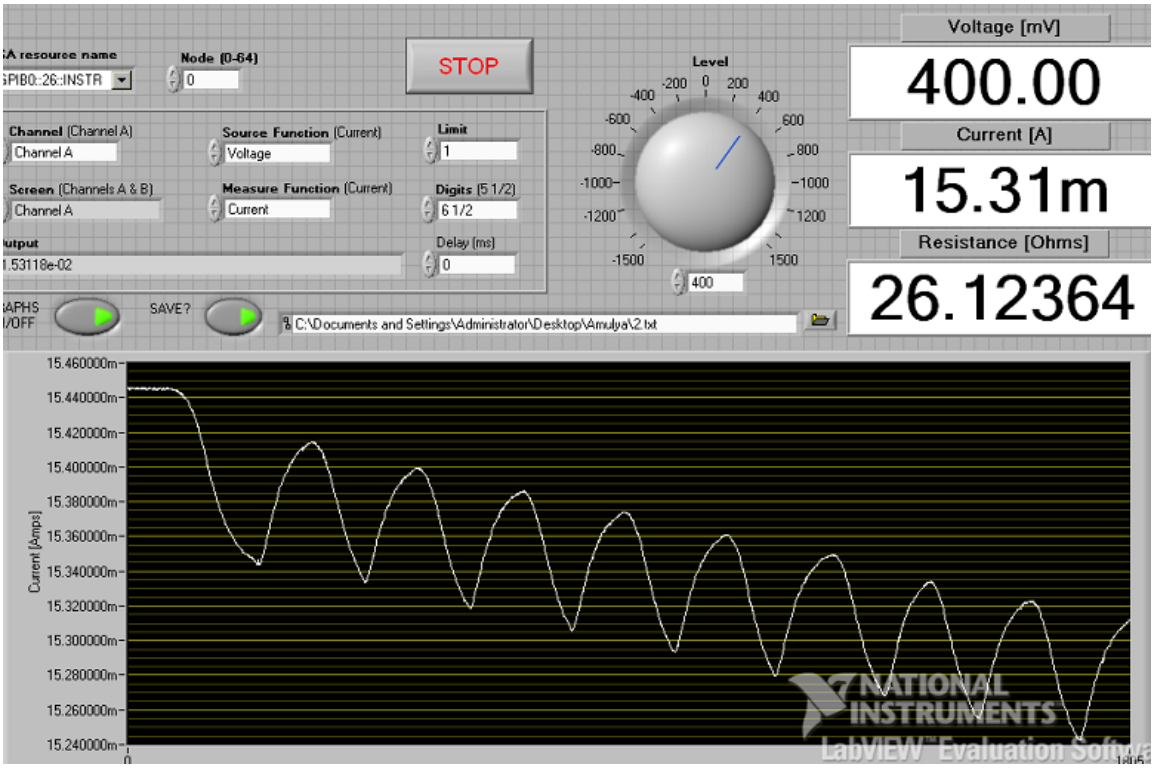

ΔI = 15.415-15.325mA = 0.09mA; ΔV = 0.09*26.13= 2.35mV; R = 664 $\frac{\mathbf{V}}{\mathbf{W}}$

b. Infrared detection data for the Palladium Bolometer with the extended Bowtie Antenna:

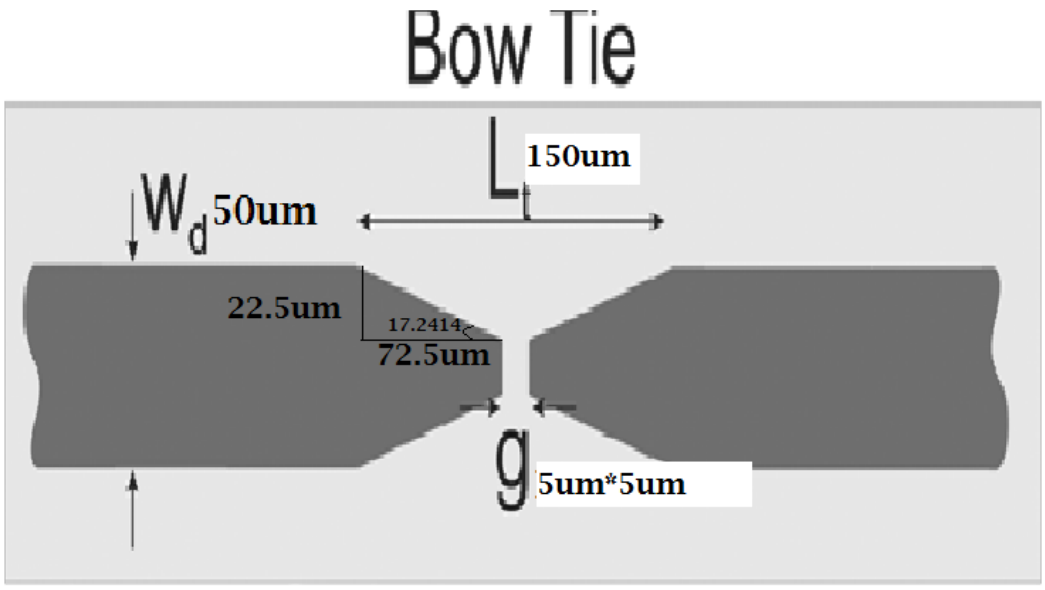

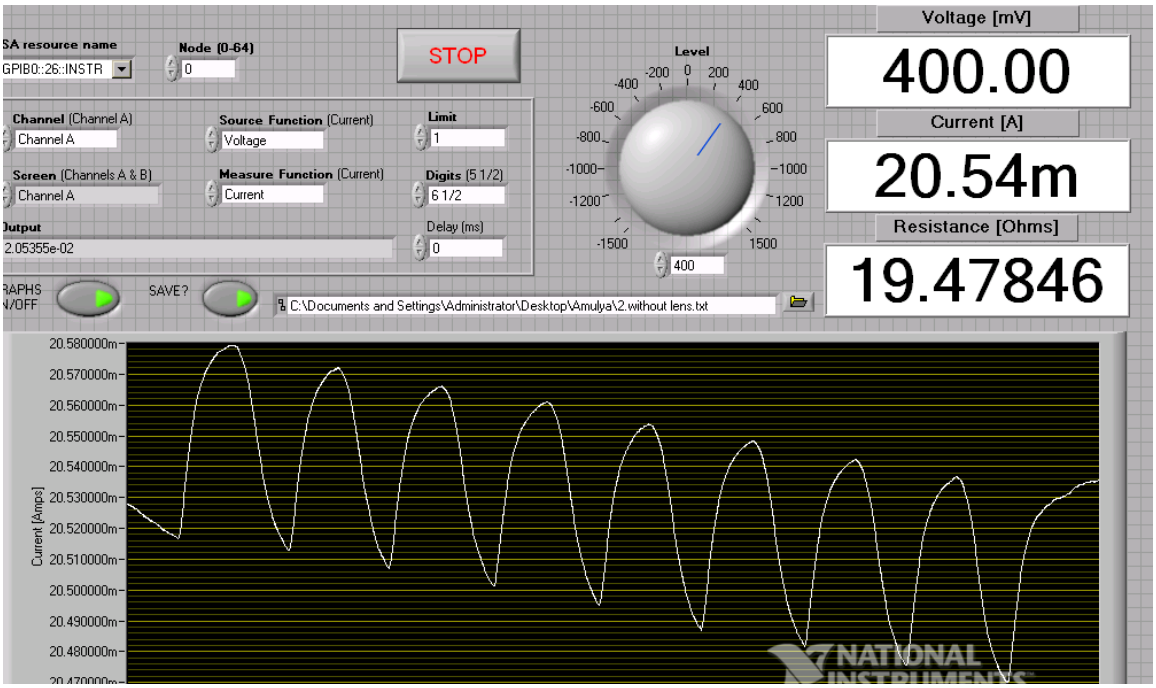

ΔI = 20.58-20.5125mA = 0.0675mA; ΔV =0.0675*19.5= 1.31625mV; R = 372$\frac{V}{W}$

REFERENCES

[1] John F Federici, Brian Schulkin, Feng Huang, Dale Gary, Robert Barat, Filipe Oliveira, David Zimdars, "THz imaging and sensing for security applications—explosives, weapons and drugs," Semiconductor Science and Technology, v20 n7 (July 2005): S266-S280

[2] W. L. Chan, J. Diebel, D. L. Mittleman. “Imaging with terahertz radiation”. Reports on Progress in Physics, v70 n8 (20070801): 1325-1379.

[3] http://cerncourier.com/cws/article/cern/28777

[4] Peter H. Siegel, “Terahertz Technology”, IEEE Transactions on Microwave Theory and Techniques, Vol 50, No 3, March 2002, pg 910-928.

[5] P. L. Richards,” Bolometers for infrared and millimeter waves”, J. Appl. Phys. 76, 1 (1994); doi: 10.1063/1.357128, Pg 1-24.

[6] D.F. Santavicca, “Bolometric Response of Superconducting Microbridges and Single-Walled carbon Nanotubes,” PhD Dissertation, Yale University, December 2009.

[7] Michael E. MacDonald and Erich N. Grossman,” Niobium Microbolometers for Far-Infrared Detection”, IEEE Transactions on Microwave Theory and Techniques, Vol.43, No 4, April 1995, Pg 893 – 896.

[8] David M Pozar,”Microwave Engineering,” John Wiley & Sons Inc, 2nd ed, ISBN: 0471170968.

[9] K. S. Yngvesson,” Very wide bandwidth hot electron bolometer heterodyne detectors based on single-walled carbon nanotubes,” Appl Phys.Lett. 87, 043503(2005); http://dx.doi.org/10.1063/1.2000330 (3 pages).

[10] Hiroshi Matsu,” Direct Detection and Interferometer Technologies in Terahertz Region”, 17th International Symposium on Space Terahertz Technology, 2006, Pg 123-126.

[11] Iulian Codreanu, Glenn D. Boreman, “Influence of dielectric substrate on the responsivity of microstrip dipole-antenna-coupled infrared micro bolometers,” 1 April 2002, Vol. 41, No. 10, APPLIED OPTICS, Pages 1835-1840

[12] Pauline Renoux, Sigurdur Ægir Jonsson, Levente J. Klein, Hendrik F. Hamann, and Snorri Ingvarsson, “Sub-wavelength bolometers: Uncooled platinum wires as infrared sensors”, 25 April 2011 / Vol. 19, No. 9 / OPTICS EXPRESS Pages 8721-8727.

[13] http://www.chemicalelements.com/elements/pd.html.

[14] Charles Kittel, “Introduction to Solid state physics”, Eighth edition, John Wiley & Sons Inc, ISBN: 047141526X.

[15] K.S. Yngvesson, “Microwave Semiconductor Devices”, Kluwer Academic, Norwell, MA (1991).

[16] Enrique Carrion, “Terahertz and Microwave detection using metallic single wall carbon nanotubes,” Master’s thesis submitted to UMass, Amherst, September 2010.

[17] Benjamin St Peter, “Terahertz imaging for cancer detection,” Master’s thesis submitted to UMass, Amherst, September 2012.

[18] Benford, Dominic J., Gaidis, Michael C., Kooi, Jacob W, “Transmission Properties of Zitex in the Infrared to Submillimeter,” Tenth International Symposium on Space Terahertz Technology, 03/1999.

[19] http://www.clippercontrols.com/pages/Dielectric-Constant-Values.html#S

[20] Daniel Koller, G. A. Ediss, Laszlo Mihaly* and G. L. Carr**, “Infrared measurements of possible IR filter materials”, International Journal of Infrared and Millimeter Waves, Vol. 27, No. 6, June 2006 (© 2007), DOI: 10.1007/s10762-006-9121-8.

[21] Nuria Llombart, Andrea Neto, “THz Time-Domain Sensing: The Antenna Dispersion Problem and a Possible Solution”, IEEE Transactions on Terahertz science and technology, VOL. 2, NO. 4, JULY 2012, Pages: 416-423.

[22] Martin M. Muthee, “Terahertz Radiation from Single Walled Carbon Nanotubes”, Master’s thesis, UMass, Amherst, August 2011.

[23] K. S. Yngvesson, "Microwave Semiconductor Devices", Kluwer Academic, Norwell, MA (1991).

[24] J.L. Hesler, T.W. Crowe, D.F. “NEP and responsivity of THz zero-bias Schottky diode detectors,” paper 1646, 32nd Intern. Conf. Infrared, Millimeter and Terahertz Waves, Sept. 2007, Cardiff, Wales.

[25] Sangwoo Kim," Room Temperature Terahertz Detection with Gallium Arsenide Field Effect Transistors via Plasmon-Assisted Self-Mixing," Ph.d thesis dessertion, University of California, Santa Barbara, Sept 2009.

[26] Eric R. Mueller "Optically pumped THz laser technology", Coherent-DEOS product note 1-10 (2001).

[27] M. C. Hersam. "Progress towards monodisperse single-walled carbon nanotubes," Nat. Nanotech., vol. 3, pp. 387-394 (2008).

[28] http://www.understandingnano.com/electrical-properties-carbon-nanotubes.html

[29] P. Avouris, Z. Chen, and V. Perebeinos, "Carbon Based Electronics," Nat. Nanotech., vol. 2, pp. 605-615 (2007).

[30] Nanotechnology For Dummies, By Earl Boysen, Nancy C. Muir, 2nd edition, published by wiley publishing Inc, page 42

[31] Bandaru PR. Electrical properties and applications of carbon nanotube structures. J Nanosci Nanotechnol 2007;7:1239–67.

[32] J. Kong, E. Yenilmez, T. W. Tombler, W. Kim, and H. Dai, "Quantum Interference and Ballistic Transmission in Nanotube Electron Waveguides," Physical Review Letters, vol. 87, No. 10, 106801, September 2001.

[33] Ji-yong Park, S. Rosenblatt, Y. Yaish, V. Sazonova, H. Üstünel, S. Braig, T. A. Arias, P. W. Brouwer, and P. J. McEuen, "Electron-Phonon Scattering in Metallic Single-Walled Carbon Nanotubes," Nano Letters, vol. 4, No. 3, pp. 517-520, 2004.

[34] F. Leonard, The Physics of Carbon Nanotube Devices, vol. 1 (William Andrew, New York, 2008)

[35] M. P .A Fisher and L. I. Glazman, "Transport in a one-dimensional Lüttinger liquid," Mesoscopic Electron Transport. Dordrecht, The Neatherlands: Kluwer, 1997

[36] P. J. Burke, "Lüttinger liquid theory as a model of the gigahertz electrical properties of carbon nanotubes," IEEE Trans. Nanotech. 1,129 (2002).

[37] J. J. Plombon et. al, "High-frequency electrical properties of individual and bundled carbon nanotubes," App. Phys. Lett., vol. 90, 063106 (2007).

[38] M. Bockrath et. al., "Lüttinger-liquid behavior in carbon nanotubes," Nature, vol. 397, pp. 598 (1999)

[39] S. Tomonaga, “Remarks on Bloch’s method of sound waves applied to many-Fermion problems,” Prog. Theor. Phys., vol. 5, no. 4, pp. 544–569, 1950.

[40] J. M. Lüttinger, “An exactly solvable model of a many-Fermion system,” J. Math. Phys., vol. 4, no. 9, p. 1154, 1963.

[41] A. E. Aliev , Infrared Phys. Technol. 2008 , 51 , 541.

[42] D. Bang , J. Lee , J. Park , J. Choi , Y. W. Chang , K.-H. Yoo , Y.-M. Huh , S. Haam , J. Mater. Chem. 2012 , 22 , 3215 .

[43] A.Y.Glamazda, V.A.Karachevtsev, W.B.Euler, I.A.Levitsky, Adv.Funct Mater2012, 22, 2177

[44] B. Pradhan, R. R. Kohlmeyer, K. Setyowati, H. A. Owen, J. Chen, Carbon 2009, 47, 1686

[45] B. Pradhan , K. Setyowati , H. Liu , D. H. Waldeck , J. Chen , Nano Lett. 2008 , 8 , 1142.

[46] M. E. Itkis , F. Borondics , A. Yu , R. C. Haddon , Science 2006 , 312 , 413.

[47] L. Xiao , Y. Zhang , Y. Wang , K. Liu , Z. Wang , T. Li , Z. Jiang , J. Shi , L. Liu , Q. Li , Y. Zhao , Z. Feng , S. Fan , K. Jiang , Nanotechnology 2011 , 22 , 025502.

[48] R. Lu , Z. Li , G. Xu , J. Z. Wu , Appl. Phys. Lett. 2009 , 94 , 163110.

[49] R. Lu , J. J. Shi , F. J. Baca , J. Z. Wu , J. Appl. Phys. 2010 , 108 , 84305.

[50] M. Mahjouri-Samani, Y.S.Zhou, X. N. He, W.Xiong, P.Hilger, Y.F.Lu , Nanotechnology 2013, 24, 035502.

[51] F. Rao, X. Liu, T. Li, Y. Zhou, Y. Wang, Nanotechnology 2009, 20, 055501 .

[52] http://www.coe.montana.edu/ee/jshaw/classes/RSS/RSS_S12/notes/6_EELE583_S12_Dets&Noise.pdf

[53] Jacob John[1], Martin Muthee[2], Maruthi Yogeesh[2], Sigfrid K. Yngvesson[2] and Kenneth R. Carter[1,] ‘Suspended Multiwall Carbon Nanotube-Based Infrared Sensors via Roll-to-Roll Fabrication’ Volume2,Issue6, pages 581–587, June 2014, DOI: 10.1002/adom.201400004.

[54] Jacob John1,2, YuYing Tang1,2, Jonathan P Rothstein2,3,James J Watkins1,2 and Kenneth R Carter1,2 'Large-area, continuous roll-to-roll nanoimprinting with PFPE compositemolds'Nanotechnology24(2013)505307(9pp),doi:10.1088/09574484/24/50/505307.online at stacks.iop.org/Nano/24/505307

[55] George Gruner, "Two-Dimensional Carbon Nanotube Networks: A Transparent Electronic Material", Mater. Res. Soc. Symp. Proc. Vol. 905E © 2006 Materials Research Society, 0905-DD06-05.1

[56] Mohammad F. Islam, Kyu Hun Kim,Youngseok Oh, Ilha Lee, "Carbon nanotube aerogels, composites including the same, and devices formed therefrom", Publication number US20140127490 A1, PCT/US2012/032229

[57] R. Lu , J. J. Shi , F. J. Baca , J. Z. Wu , J. Appl. Phys. 2010 , 108 , 84305 .

[58] R. Lu, G. Xi, and J.Z. Wu, "Effects of Thermal Annealing on Noise Property and Temperature Coefficient of Resistance of Single-Walled Carbon Nanotube Films," App. Phys. Lett. vol. 93, 213101 (2008)

[59] D. F. Santavicca , J. D. Chudow , D. E. Prober , M. S. Purewal , P. Kim ,Nano Lett. 2010, 10 , 4538

[60] U.R. Pfeiffer, and E. Ojefors, "Terahertz imaging with CMOS/BiCMOS process technologies," 36th European solid-state circuits Conference. 13–17.09 (2010).